Title

Multi-omics reveal intricate network of mitochondrial adaptations to training in human skeletal muscle

Authors

Cesare Granata[1,2,†,*], Nikeisha J. Caruana[2,3,†], Javier Botella[2], Nicholas A. Jamnick[2,4], Kevin Huynh[5], Jujiao Kuang[2], Hans A. Janssen[2], Boris Reljic[3,6], Natalie A. Mellett[5], Adrienne Laskowski[1,7], Tegan L. Stait[7], Ann E. Frazier[7,8], Melinda T. Coughlan[1,9], Peter J. Meikle[5], David R. Thorburn[7,8,10], David A. Stroud[3,‡,*] and David J. Bishop[2,‡,*]

Affiliations

[1]Department of Diabetes, Central Clinical School, Monash University, Melbourne, VIC, 3004, Australia

[2]Institute for Health and Sport (IHES), Victoria University, Melbourne, VIC, 3011, Australia

[3]Department of Biochemistry and Pharmacology and Bio21 Molecular Science and Biotechnology Institute, The University of Melbourne, Parkville, VIC, 3010, Australia

[4]Metabolic Research Unit, School of Medicine and Institute for Mental and Physical Health and Clinical Translation (iMPACT), Deakin University, Geelong, VIC, Australia

[5]Metabolomics Laboratory, Baker Heart & Diabetes Institute, Melbourne, VIC, 3004, Australia

[6]Current address: Department of Biochemistry and Molecular Biology, Monash Biomedicine Discovery Institute, Monash University, 3800, Melbourne, Australia.

[7]Murdoch Children's Research Institute, Royal Children's Hospital, Melbourne, VIC, 3052, Australia

[8]Department of Paediatrics, The University of Melbourne, Melbourne, VIC, 3052, Australia

[9]Baker Heart & Diabetes Institute, Melbourne, VIC, 3004, Australia

[10]Victorian Clinical Genetics Services, Royal Children's Hospital, Melbourne, VIC, 3052, Australia

[†]Equal contribution

[‡]Equal contribution and lead contacts

***Correspondence:** cesare.granata@monash.edu (C.G.), david.stroud@unimelb.edu.au (D.A.S), david.bishop@vu.edu.au (D.J.B)

Abstract

Defects in mitochondria have been implicated in multiple diseases and aging; therefore, interventions able to counteract these changes can improve quality of life. Exercise training is a readily accessible and inexpensive therapeutic intervention; however, the complexity of training-induced mitochondrial adaptations in skeletal muscle remains poorly understood. Here, we describe an intricate and previously undemonstrated network of differentially prioritised training-induced adaptations in human skeletal muscle mitochondria. We show that changes in hundreds of transcripts, proteins, and lipids are not stoichiometrically linked to the increase in mitochondrial content. Moreover, we demonstrate a prioritisation of specific mitochondrial functional protein networks at different stages of the training intervention, including an initial deprioritisation of oxidative phosphorylation (OXPHOS) and a prioritisation of TCA cycle and fatty acid β-oxidation linked mitochondrial respiration. This indicates that enhancing electron flow to OXPHOS may be more important to improve ATP generation in skeletal muscle than increasing the abundance of the OXPHOS machinery. Our research unearths the elaborate and multi-layered nature of the adaptive response to exercise and provides a valuable resource that can be mined to maximise the therapeutic benefits of exercise.

Key Words: mitochondrial biogenesis, mitochondrial proteome, OXPHOS, supercomplex, lipidome, transcriptome, mitochondrial respiration, electron transport chain.

Introduction

Mitochondria are the main site of energy conversion in the cell and have critical roles in other important biological processes[1]. Owing to this, defects in mitochondria have been implicated in multiple diseases, medical conditions, and aging[2-5]. The development of interventions to improve the content and function of mitochondria is therefore essential to enhance quality of life and to extend life expectancy.

Exercise training is one of the most widely accessible interventions or "therapies" to stimulate mitochondrial biogenesis[6,7]. As arguably the most extensive and also natural perturbation, exercise is also an excellent experimental model for understanding both the complex nature of mitochondrial biogenesis and the plasticity of the mitochondrial proteome in humans, which consists of more than 1300 proteins[8]. It is well accepted that exercise training induces an increase in mitochondrial content and respiratory function in skeletal muscle[9]. However, our knowledge of training-induced mitochondrial adaptations in human skeletal muscle is limited to a small fraction of the mitochondrial proteome[10], and there remain major gaps in our understanding of the magnitude, timing, and direction of change in individual mitochondrial proteins and related functional pathways.

A key biological function of mitochondria is energy conversion via oxidative phosphorylation (OXPHOS), which is carried out by the four multi-protein complexes (complexes I to IV [CI-CIV]) of the electron transport chain (ETC) and F_0F_1-ATP synthase (or CV)[11]. Assembly of the OXPHOS complexes is an intricate process requiring the coordination of two genomes (nuclear and mitochondrial) and chaperone-like proteins known as assembly factors[12]. Only two studies have investigated training-induced changes in OXPHOS complexes[13,14], reporting that exercise differentially modulates the respiratory complexes and that these changes are not always stoichiometric. Furthermore, no study has

74 investigated if training-induced changes in chaperones, assembly factors, and single
75 OXPHOS subunits occur in conjunction with, or precede, changes in the complete, functional
76 complexes. Many other processes support assembly and maintenance of the OXPHOS
77 complexes, including mitochondrial protein import and assembly pathways, mitochondrial
78 DNA transcription and translation, metabolite carriers, and pathways producing critical
79 cofactors such as coenzyme Q and iron-sulphur proteins (Fe-S)[12]. In turn, these processes are
80 reliant on pathways supporting mitochondrial biogenesis more broadly, such as lipid
81 biogenesis and maintenance of mitochondrial morphology. Whether these processes and
82 pathways are activated by exercise training and at which specific times remains unknown.
83 Moreover, whether these are affected by different training volumes, a key determinant of
84 training-induced mitochondrial adaptations[9], is also unclear.

85 Here we apply quantitative multi-omics (transcriptomics, proteomics, and lipidomics), as
86 well as bioinformatics and biochemical approaches, with a sequential exercise intervention
87 that included three different training volumes, to investigate changes within the mitochondrial
88 proteome in human skeletal muscle. We report a general increase in the expression of
89 hundreds of mitochondrial genes, proteins, and lipids that peak following the highest volume
90 of training, and which was linked with enhanced mitochondrial respiratory function and
91 supercomplex (SC) formation. A reduction in training volume led to minimal or no changes
92 in most measurements. Using biochemical and *in silico* normalisation we removed the bias
93 arising from the overall increase in mitochondrial content following training, enabling us to
94 observe novel and divergent adaptations in the mitochondrial transcriptome, proteome, and
95 lipidome that were independent of changes in overall mitochondrial content. We identified
96 almost 200 mitochondrial proteins and multiple bioenergetic, OXPHOS, and metabolic
97 pathways that were differentially regulated following changes in training volume. Our study
98 demonstrates an intricate and timely mitochondrial remodelling, expanding our fundamental

99 understanding of the steps required for training-induced mitochondrial biogenesis and leading
100 to new hypotheses regarding how training alters mitochondrial protein content and function
101 with implications for both health and disease.

Results

Increases in mitochondrial content underlie changes in supercomplex abundance and mitochondrial respiratory function following training. The traditional view of mitochondrial biogenesis proposes that an increase in mitochondrial content is required to increase mitochondrial function, and that there is a fixed stoichiometry between changes in mitochondrial content and individual mitochondrial proteins. Although this has been questioned before[15], it remains an unresolved matter. As we have previously reported a correlation between training volume and increases in mitochondrial content[9,16-18], we employed an experimental model in which ten men were sequentially exposed to different volumes (normal- [NVT], high- [HVT] and reduced- [RVT] volume training) of high-intensity interval training (HIIT) to further interrogate this paradigm (Fig. 1a). An important feature was the RVT phase, which was designed to maintain previously gained mitochondrial adaptations while reducing fatigue (referred to as tapering). A greater weekly training volume was completed during the HVT phase when compared to both the NVT and RVT phases, and also during RVT when compared to NVT (Fig. 1b). Changes in physiological and performance parameters are presented in Supplementary Table 1.

Indirect measurements of mitochondrial content[19], such as mitochondrial protein yield (Fig. 1c), citrate synthase (CS) activity (Fig. 1d), and the protein content of OXPHOS subunits assessed in whole-muscle lysates by SDS-PAGE (Fig. 1e, upper panels), increased with training volume and reached significance post-HVT. These observations are consistent with reports of training-induced increases in mitochondrial protein[6,20-22], CS activity[9], and OXPHOS subunit levels[18,23] in skeletal muscle, and with the notion that training volume is an important determinant of changes in mitochondrial content[9,16-18]. By design, RVT resulted in no change in any of these markers.

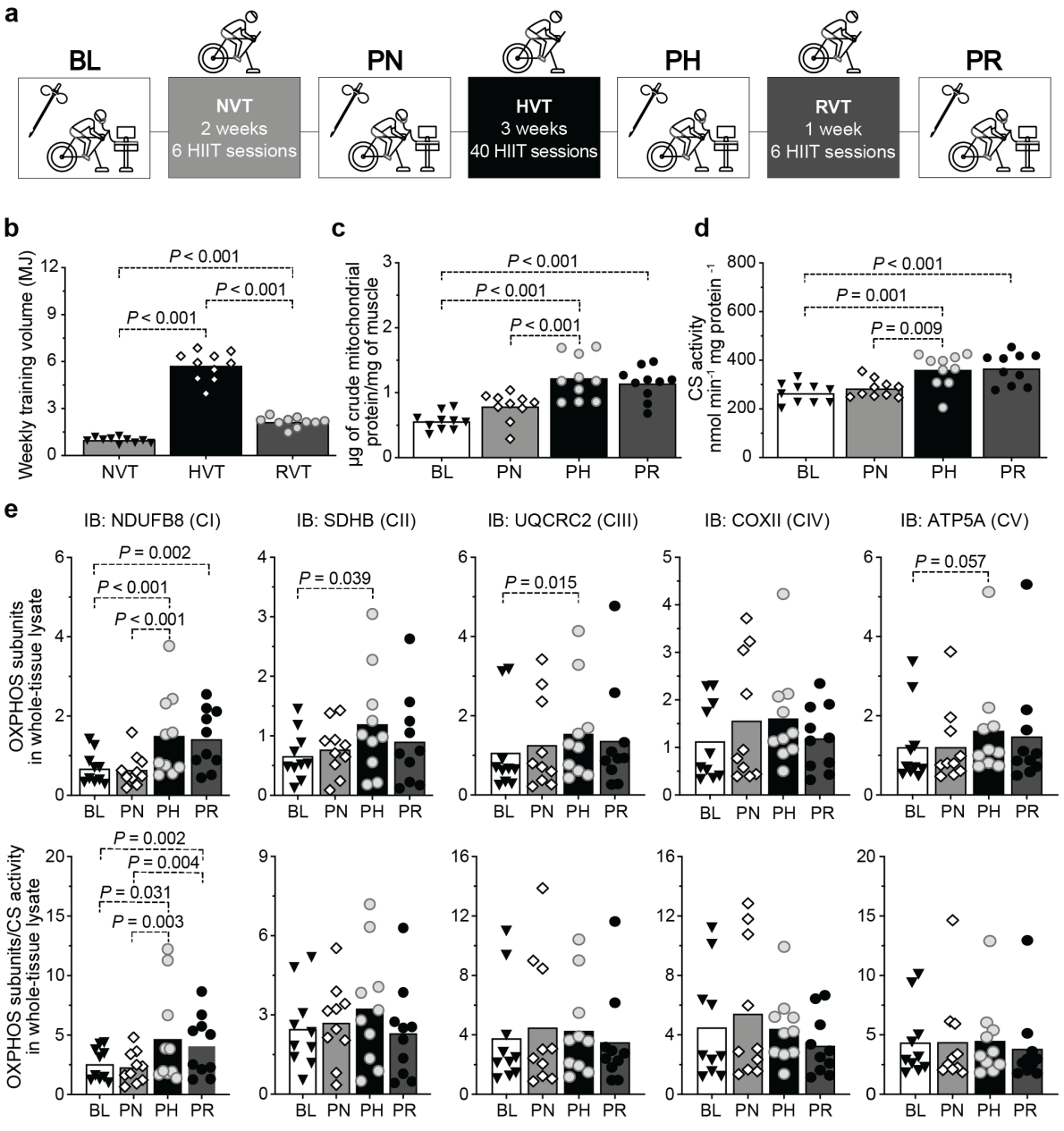

Fig 1. Exercise training increases markers of mitochondrial content in human vastus lateralis muscle in a training-volume-dependent manner. **a**, Study design. Open boxes indicate a resting skeletal muscle biopsy and testing sessions; coloured boxes indicate a training phase: NVT (normal-volume training), HVT (high-volume training), and RVT (reduced-volume training). **b**, Weekly training volume during the NVT, HVT, and RVT training phase; training volume was calculated by multiplying the absolute exercise intensity in Watts by the effective duration of exercise training in minutes (excluding the pre-training warm up and the rest period between intervals) by the total number of training sessions in each phase. **c**, Mitochondrial yield per mg of tissue achieved during mitochondria isolation of human vastus lateralis biopsy samples at different time points (biochemical mitochondrial protein enrichment). **d**, Citrate synthase (CS) enzyme activity assessed in whole-tissue (vastus lateralis) homogenates at each time point. **e**, Top panels: protein content of selected subunits of oxidative phosphorylation (OXPHOS) complexes by immunoblotting in whole-tissue (vastus lateralis) homogenates at each time point; lower panels: values from top panels

normalised by CS activity values obtained in **d**. HIIT: high-intensity interval training; MJ: megajoules; BL: baseline; PN: post-NVT; PH: post-HVT; PR: post-RVT; CI-V: complex I to V; IB: immunoblotting; ▼,◊,○, and ● represent individual values; bars represent mean values; n = 10 for all analyses; all datasets analysed by repeated measures one-way ANOVA followed by Tukey's post hoc testing. Significance: $P < 0.05$.

The activity of CS, an enzyme located in the mitochondria[24], strongly correlates with mitochondrial content (as measured by transmission electron microscopy) in human skeletal muscle[19]; therefore, to investigate the underpinnings of the training-induced changes in the OXPHOS subunits, we normalised these values by CS activity - a widely used normalisation strategy[9,18,19,25]. Following normalisation, the above changes were no longer significant, except for CI (subunit NDUFB8), indicating that, for the most part, absolute changes in OXPHOS subunits were stoichiometrically associated with the overall increase in mitochondrial content (Fig. 1e, lower panels).

In addition to increased mitochondrial content, a previous study reported that training increases the formation of respiratory chain supercomplexes (SCs)[13] - high molecular weight assemblies comprised of CI, CIII, and CIV[26] - which was suggested to contribute to improvements in mitochondrial respiration[13]. Although SCs were originally proposed to support enhanced ETC function[27], their role is controversial with multiple groups reporting that they confer no bioenergetic advantage[28]. We performed BN-PAGE analysis of SCs (Fig. 2a) to determine whether training leads to altered abundance and organisation of SCs. While we observed increases in SC abundance with increasing training volumes, achieving significance post-HVT (Fig. 2b, upper panels), this increase was no longer significant upon normalisation by CS activity (Fig. 2b, lower panels), suggesting a stoichiometric relationship between training-induced increases in mitochondrial content and SC abundance.

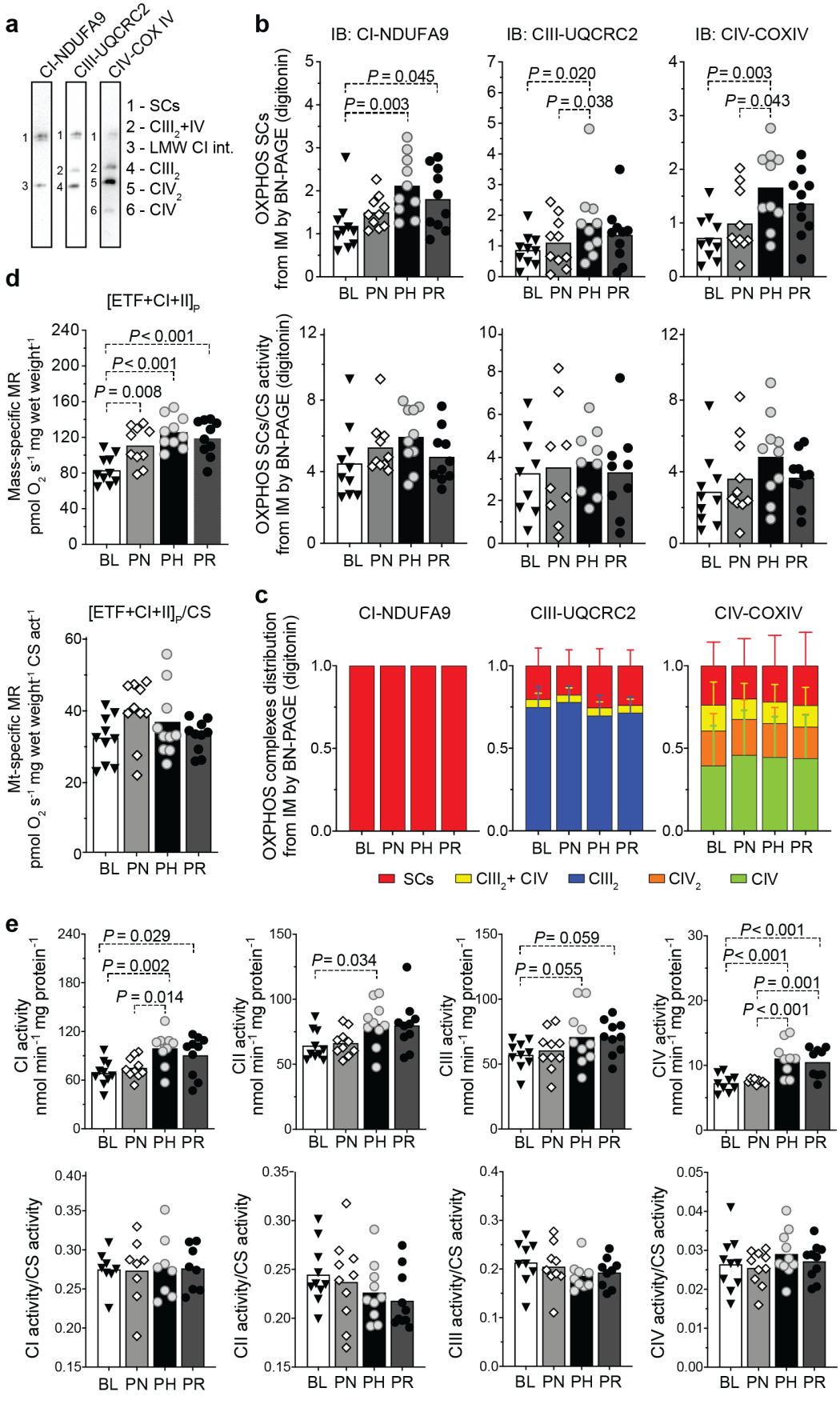

165

Fig 2. Training-induced increases in mitochondrial respiratory function and supercomplexes in human vastus lateralis muscle are driven by the increase in mitochondrial content. **a**, Representative BN-PAGE blots of isolated mitochondria (IM) fractions from human vastus lateralis muscles (images from baseline [BL] IM fractions). Band 1 (SCs): mature supercomplexes (SCs) consisting of complex I+III_n+IV_n; band 2 ($CIII_2$+IV): a supercomplex consisting of CIII and CIV; band 3 (LMW CI int): low molecular weight intermediate of CI (band not present in all samples); band 4 ($CIII_2$): CIII dimer; band 5 (CIV_2): CIV dimer; band 6 (CIV): CIV monomer. **b**, Top panels: protein content of SCs of the electron transport chain (ETC) by BN-PAGE in IM fractions from human vastus lateralis muscle biopsies at each time point (same antibodies as in **a;** antibodies probed on separate membranes); lower panels: values from top panels normalised by citrate synthase (CS) activity. **c**, Distribution of ETC complexes into SCs from images obtained in **b** at each time point. **d**, Top panel: maximal mass-specific mitochondrial respiration (MR) in permeabilized human vastus lateralis muscle fibres with convergent electron input through ETF+CI+CII ($[ETF+CI+II]_P$) at each time point; lower panel: values of mitochondrial- (mt-) specific MR, obtained after normalising values from the top panel by CS activity ($[ETF+CI+II]_P$/CS). Results for the entire substrate-uncoupler-inhibitor-titration (SUIT) protocol are shown in Supplementary Fig. 1. **e,** Top panels: enzymatic activity of ETC complexes in whole-tissue (vastus lateralis) homogenates at each time point; lower panels: values from top panels normalised by CS activity. PN: post-NVT; PH: post-HVT; PR: post-RVT; IB: immunoblotting. ▼,◊,○, and ● represent individual values; bars represent mean values; error bars in **c** represent SD; n = 10 for all analyses; datasets analysed by repeated measures one-way ANOVA followed by Tukey's post hoc testing, except for **c** (right panel) and **d** (lower panel), which were analysed by Friedman test followed by Dunn's post hoc testing, as not normally distributed. Significance: $P < 0.05$.

We next assessed whether exercise training affects the distribution of ETC complexes into SCs. In contrast to the only previous report showing a post-training redistribution of CIII and CIV (but not CI) into SCs in elderly individuals[13], our analysis revealed no significant changes following any training phase (Fig. 2c). This demonstrates that in young healthy humans HIIT does not alter the ETC complex distribution within major and minor SC assemblies. While the contrasting findings may relate to differences in the participants' average age (66 *vs.* 22 y) and baseline $\dot{V}O_{2max}$ (1.9 *vs.* 3.6 L min^{-1}), as well as the training interventions (48 sessions of moderate-intensity training in 16 weeks *vs.* 52 sessions of HIIT in 9 weeks), our results are consistent with the concept that SC assemblies are a structural feature of the ETC rather than a phenomenon conferring enhanced bioenergetics[28]. In line with this, our data indicated that the greatest changes in mitochondrial respiration (Fig. 2d and Supplementary Fig. 1, both upper panels) occurred in parallel with the greatest changes

in SC abundance (Fig. 2b, upper panels). However, following normalisation by CS activity, both of these adaptations were no longer significant except for a post-NVT increase in fatty acid-linked mitochondrial (mt-) specific respiration ([ETF]P/CS activity) (Fig. 2b, Fig. 2d, and Supplementary Fig. 1, all lower panels). Therefore, our findings do not support the hypothesis that training-induced changes in the abundance or organisation of SCs contribute to improvements in mitochondrial respiration. Instead, our data indicate that changes in mitochondrial respiration following HIIT could be largely attributed to increases in mitochondrial content. This is also supported by the observation that the greatest changes in ETC enzyme activity (Fig. 2e, upper panels) occurred in parallel with the greatest changes in markers of mitochondrial content (Fig. 1c and d), and that all of these changes were no longer significant after normalisation by CS activity (Fig. 2e, lower panels). By design, RVT resulted once again in no change in any of the above measurements.

Disentangling changes in the mitochondrial proteome from the general increase in mitochondrial content observed post-training. The above findings provide evidence that altering training volume results in a stoichiometric relationship between training-induced changes in mitochondrial content and OXPHOS subunits, SC abundance, mitochondrial respiration, and OXPHOS enzyme activity. Despite this, it remains unknown whether there is also a fixed stoichiometry between changes in mitochondrial content and individual mitochondrial proteins. To test this, we first employed RNA sequencing (RNA-seq) based transcriptomics (Supplementary Table 2). We observed the expected increase in gene transcripts encoding subunits of the OXPHOS complexes (Fig. 3a, upper panels, compare with Fig. 1e, upper panels) and enzymes of the tricarboxylic acid (TCA) cycle (Fig. 3a, central lower panel), consistent with previous studies in humans[29]; however, transcripts for genes encoding other mitochondrial proteins did not all follow the same trend (Fig. 3a, lower panels). Gene ontology enrichment analysis of all differentially expressed transcripts (Fig.

228 3b) did not identify significant alterations of pathways involved in mitochondrial respiratory
229 function (Fig. 3c; Supplementary Table 3). This reveals a greater complexity in the
230 transcriptional responses to exercise than expected; i.e., not all mitochondria-related gene
231 transcripts changed in the same direction and with a similar magnitude following different
232 training phases (Fig. 3b).

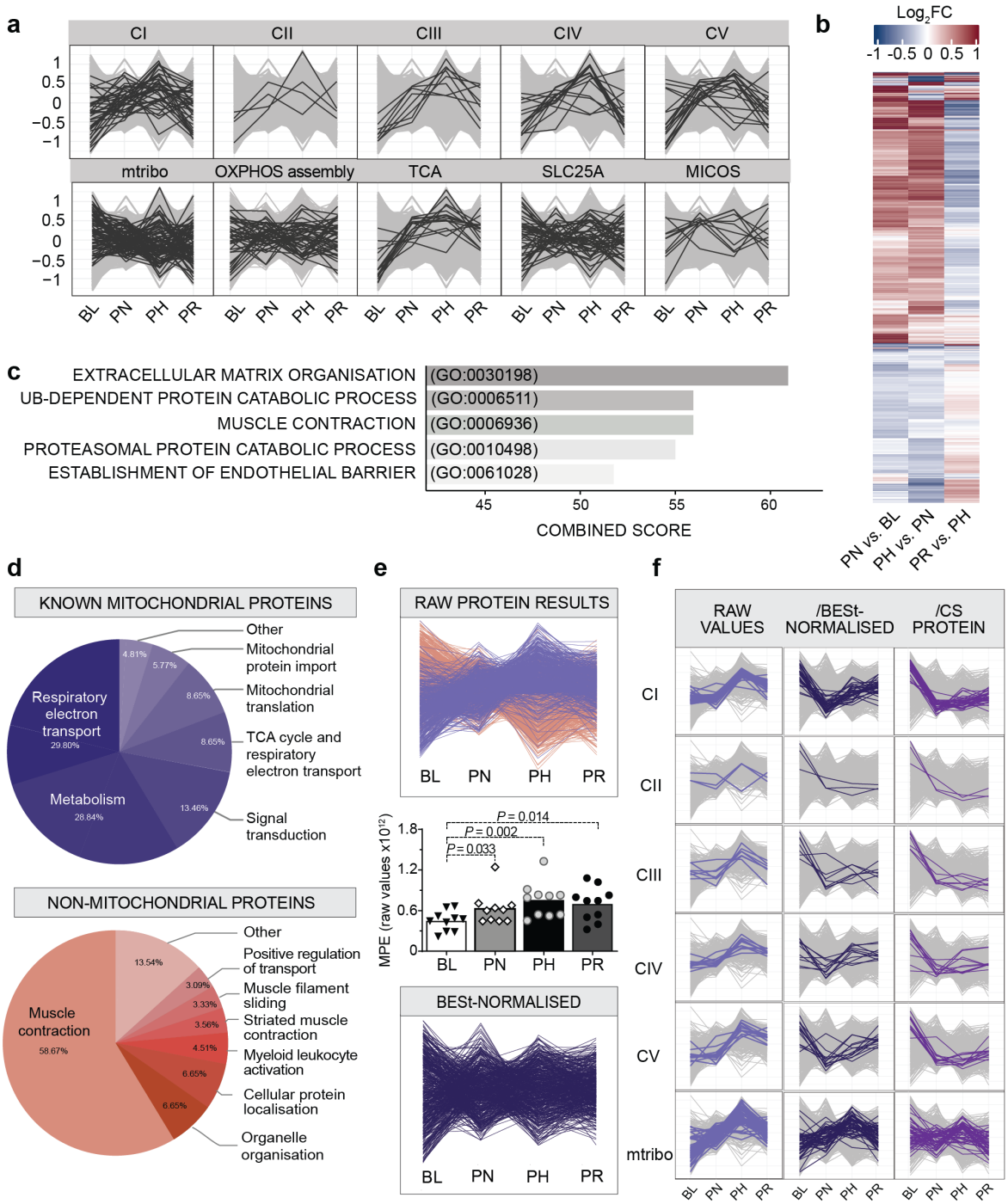

233

Fig 3. RNA-seq and raw proteomic analyses highlights training-induced changes in mitochondrial transcripts and proteins with different training volumes. a, Profile plots showing relative scaled transcripts of subunits of the five oxidative phosphorylation (OXPHOS) complexes (CI to CV), mitochondrial ribosomes (mtribo), OXPHOS assembly, TCA cycle, SLC25As and mitochondrial contact site and cristae organising system (MICOS) complex. Transcripts were grouped according to known literature (see methods). **b**, Heatmap of differentially expressed transcripts between training phases determined with an adjusted $P < 0.05$ (Benjamini Hochberg). Row clustering determined by unsupervised hierarchical cluster analysis. **c**, Biological process (BP) gene ontology of all differentially expressed transcripts as in **b**; the five terms with the highest combined score, as determined by *Enrichr* (see methods), are displayed. **d**, Pie charts showing the relative enrichment terms, as determined by *Reactome*, of "known mitochondrial" and "non-mitochondrial" proteins, identified by the Integrated Mitochondrial Protein Index (IMPI) database ("Known Mitochondrial") from isolated mitochondria (IM) fractions. **e**, Training-induced differences in the mitochondrial protein content of IM fractions. Upper panel: profile plot of all non-normalised (raw) intensity values displaying "known mitochondrial" (IMPI "Known Mitochondrial") (magenta) and non-mitochondrial (salmon) proteins co-precipitating during mitochondrial isolation. Proteins identified in less than 70% of samples were removed. Middle panel: mitochondrial protein enrichment (MPE) obtained by adding the raw intensity values from LC-MS/MS analysis of all "known mitochondrial" proteins (IMPI "Known Mitochondrial") at the four different time points. ▼,◊,○, and ● represent individual values; bars represent mean values; analysed by repeated measures one-way ANOVA followed by Tukey's post hoc testing. Significance: $P < 0.05$. Lower panel: same as upper panel but following removal of non-mitochondrial proteins and statistical correction (BESt-) normalisation. **f**, Scaled profile plots showing the relative abundance of subunits of OXPHOS complexes and mtribo of the raw intensity values of "known mitochondrial" proteins (IMPI "Known Mitochondrial") following valid value filtering (left panels), and values obtained after BESt-normalisation (central panels), or after normalisation by the protein content of citrate synthase (CS) from the proteomics analysis (right panels). BL: baseline; PN: post-NVT; PH: post-HVT; PR: post-RVT. n = 5 for **a**, **b**, and **c**, n = 10 for all other analyses.

As transcriptomics suggested there may not be a fixed stoichiometry between training-induced changes in mitochondrial content and individual mitochondrial proteins, we sought to confirm this by quantitative proteomics. To negate the general increase in mitochondrial content following exercise training and avoid this inherent bias on our proteomics measurements, we performed label-free quantitative (LFQ) proteomics on equal amounts of protein isolated from biopsies using differential centrifugation (biochemical enrichment). We quantified 1,411 proteins - 726 of which were annotated as mitochondrial based on either the Mitocarta2.0[30] or Integrated Mitochondrial Protein Index (IMPI; Known and Predicted Mitochondrial)[8] databases (Supplementary Table 4). Considering only the high-confidence

IMPI (Known Mitochondrial) dataset[8] (584 annotated mitochondrial proteins), mitochondrial proteins represented 41% of the total number of proteins identified in our mitochondrial isolates, contributing to 32% of the overall protein abundance based on raw intensity data for each protein (Supplementary Table 4). This indicated the presence of a significant proportion of non-mitochondrial proteins following mitochondrial isolation.

To better characterise our mitochondrial isolates, we performed separate enrichment analyses on both the high-confidence mitochondrial proteins (IMPI Known Mitochondrial[8]) and the remaining proteins detected across all samples. While known mitochondrial proteins were enriched in mitochondrial ontologies as expected, other proteins co-isolating with mitochondria were predominantly of myofibrillar origin (Fig. 3d), consistent with most mitochondria in skeletal muscle being tightly associated with myofibrils[31]. This suggests that increases in mitochondrial proteins observed with training (Fig. 3e, upper panel, magenta profiles) may result from differences in mitochondrial protein enrichment (MPE) - the contribution of mitochondrial protein intensities relative to all protein intensities - in our mitochondria isolates at different time points (e.g., greatest MPE post-HVT). Indeed, the MPE for the 4 different time points was significantly different (Fig. 3e, middle panel) and corresponded to 24.5% at baseline (BL), 31.5% post-NVT (PN), 39.3% post-HVT (PH), and 34.5% post-RVT (PR) (Supplementary Table 4) - a pattern consistent with our assessment of mitochondrial content (compare Fig. 3e, middle panel with Fig. 1c and d). This confirmed the training-induced increase in mitochondrial proteins and demonstrated that the MPE in our biochemically enriched mitochondrial isolates changed with training. To eliminate the bias arising from different MPEs across time points, we complemented our biochemical enrichment approach with a statistical correction strategy consisting of *i*) removing proteins that were identified in less than 70% of samples, *ii*) sub-setting the known mitochondrial proteins from the non-mitochondrial proteins, and *iii*) undertaking variance stabilising

298 normalisation (VSN) to reduce variation between human participants (see methods for more
299 detail). This resulted in the retention of 498 mitochondrial proteins quantified across the
300 dataset with high confidence (Supplementary Table 5). Importantly, unlike CS activity, which
301 is a single value for each sample, our normalisation method utilises the trends of hundreds of
302 proteins and reduces the confounding effect of potential outliers. Plotting the resulting data
303 revealed that the general increase in mitochondrial proteins with different training volumes
304 had been compensated for, indicating that our biochemical enrichment and statistical
305 correction (BESt-normalisation) was successful (Fig. 3e, lower panel). In further support of
306 our normalisation strategy, principal component analysis showed good segregation of
307 samples corresponding to the different time points (Supplementary Fig. 2a, left panel).

308 Proteomics analysis of non-normalised intensity values revealed an increase in the relative
309 abundance of OXPHOS subunits in the mitochondrial isolates after the first two training
310 phases, and a decrease post-RVT (Fig. 3f, left panels). Moreover, this provides evidence of a
311 coordinated training-induced adaptation as almost all of the 78 OXPHOS subunits identified
312 changed in a concerted fashion during training. An advantage of our BESt-normalisation is
313 that it enabled an unbiased comparison of the changes in individual mitochondrial proteins
314 relative to the overall increase in mitochondrial content following different training phases.
315 Following BESt-normalisation, the content of OXPHOS subunits exhibited discreet and
316 specific changes in response to different training volumes, including a generalised post-NVT
317 decrease (Fig. 3f, central panels; results discussed in more detail later). Similar results were
318 obtained when normalising proteomics data by the protein content of CS derived by
319 proteomics assessment (Fig. 3f, right panels), and when normalising SDS-PAGE immunoblot
320 intensities of OXPHOS subunits detected in mitochondrial isolates by CS activity
321 (Supplementary Fig. 2b). In contrast, even after BESt-normalisation, the levels of
322 mitochondrial ribosomal subunits increased both post-NVT and post-HVT and decreased

post-RVT (Fig. 3f, central panels). Taken together, these results demonstrate the absence of a fixed stoichiometry between training-induced changes in individual mitochondrial proteins and overall mitochondrial content.

From this point onwards, unless specified otherwise, post BESt-normalisation proteomics results will be presented, enabling the investigation of training-induced changes in mitochondrial proteins without the influence of the overall increase in mitochondrial content.

Discovery of novel mitochondrial proteins and functional classes differentially affected by exercise training. We next interrogated our BESt-normalised mitochondrial proteome to better understand non-stoichiometric changes in individual mitochondrial proteins to different training volumes. We performed an ANOVA and identified 185 mitochondrial proteins that were differentially expressed across the three training phases (Supplementary Table 6). This is far greater than the number of proteins previously reported to change post-training in human skeletal muscle[31-34] (Supplementary Fig. 2c). Unsupervised hierarchical clustering of all differentially expressed mitochondrial proteins revealed six clusters with distinct patterns of change in response to training (Fig. 4a; Supplementary Fig. 3a). These findings confirm the absence of a fixed stoichiometry between training-induced changes in individual mitochondrial proteins.

Enrichment analysis of differentially expressed proteins within each cluster revealed these to be enriched in, but not always exclusively contain, proteins involved in fatty acid β-oxidation (FAO), mitochondrial translation, the TCA cycle, OXPHOS, metabolism of amino acids, and cristae formation, respectively (Supplementary Fig. 3b; Supplementary Table 6). Because not all proteins belonging to each individual Reactome pathway segregated within one cluster (Supplementary Fig. 3c), we compared our 185 differentially expressed proteins with proteins

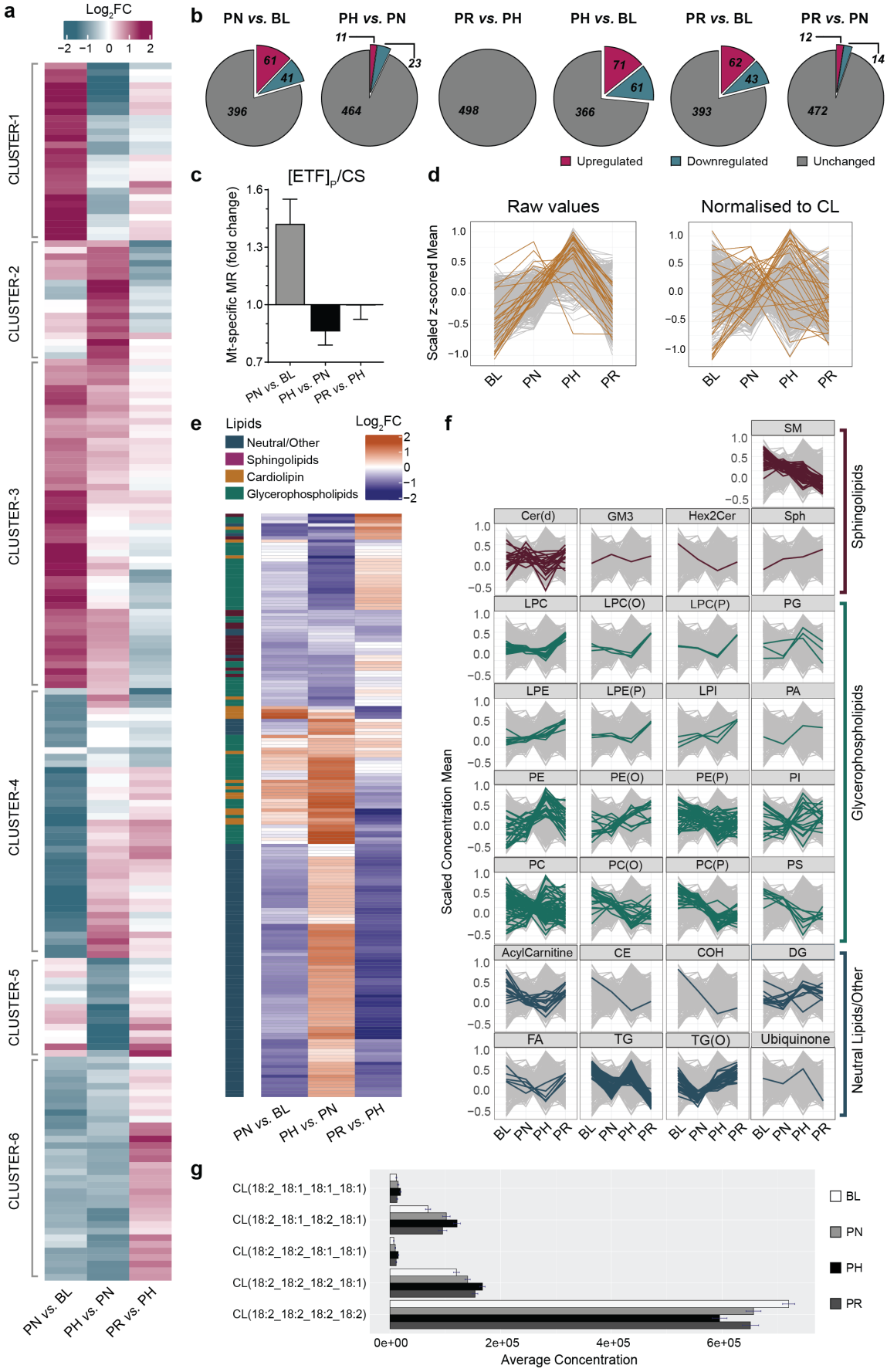

346

Fig 4. Training-induced differential prioritisation and non-stoichiometric adaptations in the proteome and lipidome. **a**, Heatmap of BESt-normalised differentially expressed mitochondrial proteins (IMPI "Known Mitochondrial") between training phases determined with an adjusted $P < 0.01$ (Benjamini Hochberg). Row clustering determined by unsupervised hierarchical cluster analysis. **b**, Venn diagram representations of the number of BESt-normalised differentially expressed mitochondrial proteins (IMPI "Known Mitochondrial") between each of the time points. Differentially expressed proteins for each time point comparison were identified by linear modelling with an adjusted P value < 0.01 using the Benjamini Hochberg method (Supplementary Table 8). **c**, Mitochondrial- (mt-) specific respiration (obtained by normalising the equivalent value of mass-specific mitochondrial respiration [MR] by citrate synthase [CS] activity) in permeabilized human vastus lateralis muscle fibres with electron input through ETF via addition of octanoylcarnitine and pyruvate; data derived from the substrate-uncoupler-inhibitor titration (SUIT) protocol shown in Supplementary Fig. 1. **d**, Left panel: all-lipids profile plot of non-normalised (raw) intensity values from mitochondrial isolates displaying all individual CL species (gold) and all other lipid species (grey) at each time point. Right panel: same as left panel after normalisation by the entire CL class. **e**, Heatmap of differentially expressed lipids after normalisation by the entire CL class between training phases determined with an adjusted $P < 0.05$ (Benjamini Hochberg). Row clustering determined by unsupervised hierarchical cluster analysis. **f**, Profile plots of the scaled concentration mean of different lipid classes. For each profile plot, all the individual lipid species identified within the specific class are represented in colour over the entire lipidome (grey) at each time point. The intensity values for all lipid species were normalised by the entire CL class to adjust for changes in mitochondrial content. **g**, The 5 most abundant CL species that were differentially expressed as determined in **e**; the complete list of differentially expressed CL species is shown in Supplementary Fig. 4b. BL: baseline; PN: post-NVT; PH: post-HVT; PR: post-RVT. n = 10 for all analyses.

belonging to the pathway protein list (Reactome R-HSA) associated with each of the above six pathways (Supplementary Table 7); matching proteins were used to generate the individual pathway heatmaps presented in Fig. 5 and have been used to discuss our findings in the results section. These pathway heatmaps also included other proteins known to be involved in the specific pathway of interest identified through literature but absent in the Reactome pathway protein list (see methods for more information); moreover, pathways other than the aforementioned six were also investigated. Proteins involved in two or more pathways were either presented in both pathways or were assigned to the pathway involving the protein's primary function and/or most closely matching their training-induced changes. To pinpoint the origin of training-induced changes in individual mitochondrial proteins, we performed unpaired t-tests between group pairs following permutation-based false discovery

rate (FDR) correction. Using a conservative approach, we matched the differentially expressed proteins identified by each t-test comparison with the 185 differentially expressed proteins identified by the ANOVA (Supplementary Table 8). The majority of changes occurred during the initial NVT phase (Fig. 4b; Supplementary Table 8), where 102 proteins were differentially expressed, suggesting that the greatest number of mitochondrial adaptations took place within the first few training sessions and they became harder to obtain as the training progressed (Fig. 4a, note the strongest changes are found in the "PN *vs.* BL" column). Our study also confirms that the training stimulus during the RVT phase was sufficient to prevent loss of adaptations (Fig. 4b; Supplementary Table 8).

Proteins important for the translation of mitochondrial proteins are sensitive to training volume. We next examined the six over-represented pathways highlighted by our enrichment analysis, beginning with the pathway related to mitochondrial protein translation (Fig. 5), which mostly segregated within cluster-2 (Supplementary Fig. 3b and c; Supplementary Table 6). Specifically, we identified proteins from both the small 28S (MRPS5, MRPS22, MRPS27) and large 39S (MRPL4, MRPL18) subunits of the mitochondrial ribosome, as well as proteins involved in translation initiation (MTIF2) and elongation (GFM1, PTCD3, TSFM, TUSM) (Fig. 5). Whereas only four proteins were upregulated post-NVT, eight of the 10 aforementioned proteins were upregulated post-HVT, with six remaining elevated post-RVT (Supplementary Table 8). To the best of our knowledge, this is the first study to directly demonstrate training-induced changes in these or related mitochondrial translation proteins in young, healthy humans, as previous research reported training-induced increases in older (65 to 80 years), but not younger (18 to 30 years), individuals[34]. Our findings also indicate that changes in proteins involved in mitochondrial protein translation are sensitive to training volume, consistent with a study observing a positive association between these proteins and physical activity levels in healthy individuals (20 to 87 years)[35].

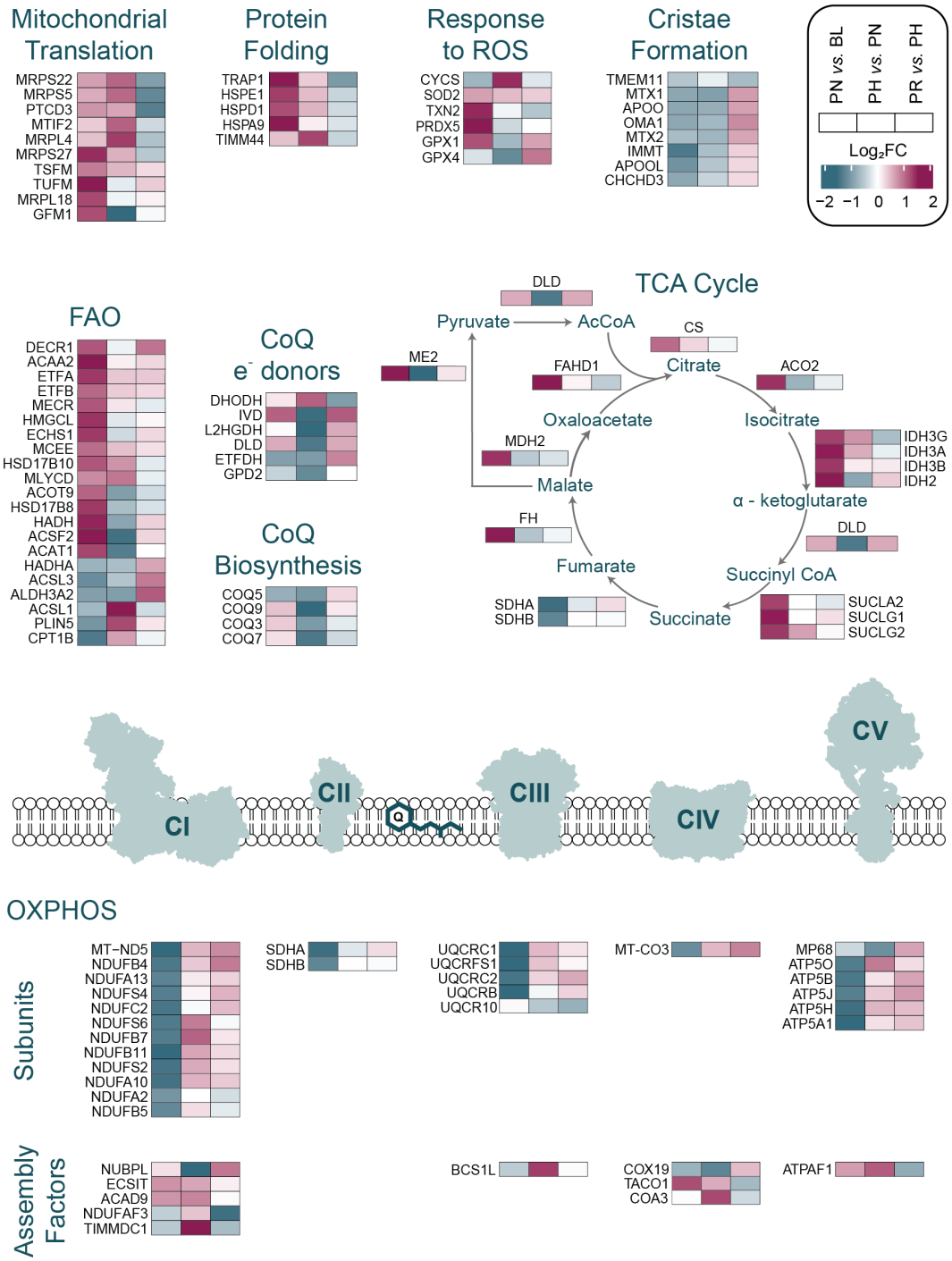

410

411 **Fig 5. Overview of training-induced changes in mitochondrial protein functional classes**
412 **and metabolic pathways**. Protein functional classes and/or metabolic pathways (defined in
413 Supplementary Table 7) as determined in Supplementary Table 8. Row clustering determined
414 by unsupervised hierarchical cluster analysis. BL: baseline; PN: post-NVT; PH: post-HVT;
415 PR: post-RVT; ROS: reactive oxygen species; FAO: fatty acid β-oxidation; CoQ: Coenzyme
416 Q; TCA: tricarboxylic acid cycle; OXPHOS: oxidative phosphorylation.

Mitochondria prioritise the TCA cycle and FAO in response to NVT. Proteins involved in the TCA cycle pathway grouped mainly within cluster-3 and, to a lesser extent, cluster-1 (Supplementary Fig. 3b and c; Supplementary Table 6). This pathway was characterised by a large and concerted increase post-NVT (12 of 16 enzymes were significantly increased), with many of these proteins remaining upregulated compared to BL both post-HVT and post-RVT (Fig. 5, Supplementary Table 8). Of note, SDHA and SDHB, subunits of CII - the only TCA cycle enzyme that also participates in the ETC - clustered with the majority of OXPHOS subunits (discussed below) and decreased during NVT. While training-induced changes in some TCA cycle proteins have been reported[31,33], this is the first study to reveal training-induced increases in ACO2, SUCLG1, SUCLG2, SUCLA2, and FAHD1, and that these enzymes adapted mostly in a coordinated fashion.

Proteins involved in FAO segregated mainly within cluster-1 and cluster-3 (Supplementary Fig. 3b and c; Supplementary Table 6). Our data demonstrated a large and concerted increase in these proteins post-NVT, with minimal (HVT) and no (RVT) changes thereafter (Fig. 5; Supplementary Table 8). Proteins increased post-NVT included chain shortening enzymes involved in FAO (ACAA2, ACSF2, ECHS1, HADH, HSD17B10, MECR, MLYCD) and enzymes required to convert unsaturated fatty acids into intermediates of FAO (DECR1 and HSD17B8). Similar increases were also observed for ETFA and ETFB, which transfer electrons produced during FAO to the OXPHOS system. These findings demonstrate an early increase in FAO, as confirmed by the post-NVT increase in FAO-linked mt-specific respiration ([ETF]$_P$/CS, Fig. 4c). These results are also consistent with previous reports observing training-induced increases in FAO-linked mitochondrial respiration after as few as six training sessions[9,36,37]. HMGCL and ACAT1, two enzymes involved in the ketogenesis pathway, were also increased, possibly suggesting that excess acetyl-CoA generated by accumulative FAO may be fed into ketogenesis. Taken together, these findings indicate that

the synthesis of proteins involved in both the TCA cycle and FAO pathways is prioritised in the early stages of an HIIT intervention; these increases may have contributed, at least in part, to the training-induced increase in mitochondrial respiration (Supplementary Fig. 1, upper panels).

Lipidomics highlights a divergent response to training of different lipid classes. To highlight specific changes in fatty acid composition, LC-MS/MS based comparative lipidomics was performed using the same mitochondrial isolates used for proteomics. A total of 779 species representing 30 lipid classes (Supplementary Table 9) were quantified. Changes in cardiolipins (CLs), an essential component for optimal mitochondrial structure and bioenergetics[38], mirrored changes in training volume and in non-normalised mitochondrial proteins (compare Fig. 4d, left panel with Fig. 3e, upper panel; Supplementary Table 9). Indeed, CL is the biomarker most strongly associated with mitochondrial content in human skeletal muscle[19]; therefore, to ensure that our lipidomics data were corrected for changes in MPE in our fractions, we applied a similar approach to the one used for proteomics where lipidomic results were normalised according to the trend observed for the CL class (see methods). Post-normalisation profile plots of CL species indicated that, despite changes in individual CL species, the general increase in mitochondrial content with different training volumes had been compensated for by our normalisation strategy (Fig. 4d; right panel), and the lipid profiles could be used to readily segregate samples according to training volume (Supplementary Fig. 2a, right panel). From this point on we will present lipidomics results obtained post normalisation, unless specified otherwise.

We identified a total of 182 differentially expressed lipid species (Fig. 4e; Supplementary Table 10). Similar to proteomics, and consistent with previous research in humans[39,40], our study highlighted the divergent response to training of different lipid classes and species

relative to overall changes in mitochondrial content (compare Fig. 4f with Supplementary Fig. 3a). However, in contrast to proteomics, where the greatest number of changes was observed early (during NVT) and no changes were observed during RVT, our lipidomics assessment showed no significant changes during NVT, but changes during RVT, with the greatest number observed during HVT (Supplementary Fig. 4a), possibly suggesting a delayed response in lipids compared to proteins. In general, training-induced changes in lipid species were mainly related to mitochondrial membrane-based lipids (CLs, phosphatidylethanolamines and phosphatidylcholines) and the triglycerides (TGs) (Supplementary Fig. 4a). Contrary to previous training studies in obese humans[39-41], we did not observe reductions in muscle ceramides [with the exception of Cer(d18:1/18:0) during HVT] or diacylglycerol content in our healthy, young men following training. While this could indicate a different response of lipid species in mitochondria isolates (our study) compared to whole-muscle lysates[39-41], as previously suggested[42], it could also highlight adaptation differences between obese and healthy individuals.

Of relevance to the increase in FAO reported above, we observed a post-NVT decrease in TGs (Fig. 4f), a class of lipids used as an important source of energy production during exercise[43]; however, likely due to the high number of multiple comparisons in our bioinformatic analysis (n = 779), no significant changes in single TG species were detected (Supplementary Fig. 4a). The decrease in TGs in our study is likely indicative of an increase in fatty acid turnover, which would be consistent with the reported post-NVT increase in both FAO enzymes (Fig. 5) and FAO-linked mt-specific respiration (Fig. 4c). Finally, changes in TGs (Fig. 4f), which are not found in mitochondria but rather in lipid droplets[44], mirrored changes in PLIN5 (Fig. 5). Since PLIN5 is a protein that tethers mitochondria to lipid droplets and regulates the release of lipids for FAO[45,46], we hypothesise that training-induced changes in TGs may indicate changes in association of lipid droplets with mitochondria.

While few studies have evaluated the effects of different training interventions on skeletal muscle lipid species, our results add to the growing evidence that changes with training are specific to the exercise prescription and that training volume is also an important determinant of changes in lipid species.

Synthesis of OXPHOS subunits is not a priority in the early adaptations to HIIT. We next examined the OXPHOS pathway, which segregated almost entirely in cluster-4 (Supplementary Fig. 3b and c; Supplementary Table 6). We report training-induced changes in 26 OXPHOS subunits (Fig. 5), equivalent to ~33% of all subunits identified, most for the first time. Differentially expressed OXPHOS proteins included subunits from all six of the modules required for the assembly of CI, both catalytic subunits of CII, as well as subunits from CIII, one of the three core subunits of CIV, and proteins found in both functional domains of CV. Specifically, we observed a large and coordinated (23 subunits) decrease post-NVT, with no changes during HVT and/or RVT (Fig. 5; Supplementary Table 8). Changes in SLC25A4 (ANT1), a protein catalysing the exchange of cytosolic ADP and mitochondrial ATP across the mitochondrial inner membrane[47], mirrored these changes (Supplementary Table 8). The post-NVT decrease in OXPHOS subunits indicates that during times of increased biogenesis the synthesis of proteins involved in pathways other than OXPHOS is prioritised. The number of OXPHOS subunits that were significantly decreased compared to BL was reduced as the training progressed (23, 14, and 8 for post-NVT, post-HVT, and post-RVT, respectively). Indeed, our results demonstrated a large post-NVT increase in TCA cycle and FAO related enzymes, the major providers of reducing equivalents (NADH and $FADH_2$) to the OXPHOS system[48]; this suggests that enhancement of these two metabolic pathways may be more important to increase mitochondrial respiration following exercise training (Supplementary Fig. 1, upper panels) than an increase in OXPHOS subunits. However, an increase in reducing equivalents coupled with the de-prioritisation of the

OXPHOS machinery could lead to increased reactive oxygen species (ROS) generation. Here we report an immediate post-NVT increase in the abundance of enzymes involved in protection from oxidative stress, such as PRDX5 (the most increased protein), TXN2, and GPX1[49] (Fig. 5; Supplementary Table 8). Moreover, both SOD2, the mitochondrial ROS scavenger[49], and PRDX5 were increased post-HVT and post-RVT. This suggests that training-induced synthesis of proteins involved in the protection from oxidative stress was emphasised early during the training intervention and maintained throughout, consistent with the notion that exercise training provides protection against oxidative stress[49,50].

The coordinated assembly of OXPHOS complexes involves various assembly factors, chaperones, and protein translocation components, and has been suggested to be in the order of days[51]. Whereas increases in OXPHOS assembly factors occurred mostly post-HVT (Fig. 5; Supplementary Table 8), changes in subunits of the mitochondrial ribosome (Fig. 3f, lower central panel), which synthesise the 13 OXPHOS subunits encoded by mitochondrial DNA, and in several chaperone proteins regulating import and folding of proteins destined for the mitochondrial matrix, took place earlier (post-NVT; Fig. 5; Supplementary Table 8). Chaperone proteins upregulated post-NVT included HSPA9 (mtHSP70), HSPD1 (mtHSP60), HSPE1 (mtHSP10), and TRAP1 (mtHSP90), whereby TIMM44 was increased during HVT (Fig. 5; Supplementary Table 8). All five proteins remained elevated compared to BL both post-HVT and post-RVT. Except for HSPE1[31], none of the above chaperones has previously been reported to respond to exercise. All of these chaperones are known to interact[52], which suggests a coordinated increase in the protein quality control system in response to exercise training. While we detected many subunits of the translocases of the outer and inner membrane (TOM and TIM, respectively; Supplementary Table 4), which are required for importing nuclear-encoded subunits[53], most did not significantly change with training,

suggesting that their levels remain stable and are sufficient to support training-induced increases in mitochondrial biogenesis.

Given the importance of CLs for the assembly and stability of mitochondrial membrane protein complexes and respiratory chain SCs[54,55] we again interrogated our normalised mitochondrial lipidome. We observed a remodelling of CL composition (Fig. 4g; Supplementary Fig. 4b). Notably, following NVT and HVT, we observed a decrease in the abundance of tetra-linoleoyl CL (18:2_18:2_18:2_18:2), the dominant form of CLs found in skeletal muscle[56]. Accompanying this were concomitant increases in CLs containing oleic acid (18:1) and to a lesser extent palmitoleic acid (16:1) acyl chains (Fig. 4g; Supplementary Fig. 4b). This may reflect a lack in relative availability of dietary linoleic acid due to increased mitochondrial biogenesis, since the nature of CL remodelling catalysed by TAZ, which was unaltered in our dataset, appears to be controlled predominantly by lipid availability[57]. This compensation in CL content is in line with our observation that increased training volume does not lead to changes in respiratory chain SC assembly (Fig. 2c) or the content-normalised OXPHOS enzyme activities we observed post-NVT and post-RVT (Fig. 2e, lower panels).

Coenzyme Q biosynthesis and cristae formation are not prioritised during high-volume HIIT. Despite enrichment analysis suggesting cluster-5 to be enriched in metabolism of amino acids and derivatives, upon further inspection we identified this cluster to predominantly contain proteins involved in the biosynthesis and function of coenzyme Q (CoQ or ubiquinone; Supplementary Fig. 3b and c; Supplementary Table 6) - an enzyme with an essential role as an electron transfer lipid in OXPHOS processes[58]. We identified changes in four constituents (COQ3, COQ5, COQ7, COQ9) of the CoQ synthome (Fig. 5; Supplementary Table 7), a multi-subunit complex necessary for the biosynthesis of CoQ[59].

564 We report no changes post-NVT, consistent with previous research investigating the effects
565 of short-duration (< 3 weeks) exercise training on CoQ content in human skeletal muscle[60].
566 However, post-HVT we report a concerted reduction in three of these proteins, which also
567 persisted post-RVT (Supplementary Table 8). This indicates that CoQ biosynthesis is not
568 prioritised in response to high-volume HIIT, suggesting that enhancing the CoQ pool may not
569 be a priority to support the increase in mitochondrial respiration in human skeletal muscle.

570 CoQ is an electron carrier shuttling electrons derived from the TCA cycle (via CI and CII),
571 pyrimidine biosynthesis (via DHODH), glycolysis (via GPD2), and FAO (via EFTDH) to
572 Complex III[48]. Moreover, other enzymes located near or on the inner mitochondrial
573 membrane feeding electrons to CoQ, such as IVD[61], DLD[62], and L2HGDH[63], were also
574 identified in our study (Supplementary Table 7). Similar to the decrease reported above in CI
575 and CII subunits post-NVT, we report decreases in four of these enzymes during HVT, with
576 three of them remaining downregulated both post-HVT and post-RVT; conversely, IVD was
577 increased during NVT and DHODH was elevated post-HVT (Fig. 5; Supplementary Table 8).
578 The lack of a clear correlation between the content of the above proteins and that of CoQ may
579 be ascribed to changing preferences for energy utilisation over the course of the training
580 intervention, as also indicated by the differential prioritisation of the various metabolic
581 pathways described above.

582 The mitochondrial contact site and cristae organising system (MICOS) is pivotal for the
583 formation of cristae junctions, providing the extended membrane surface hosting OXPHOS
584 complexes[64]. The MICOS associates with the outer membrane sorting and assembly
585 machinery (SAM) to yield the mitochondrial intermembrane space bridging complex (MIB),
586 thus linking the mitochondrial inner and outer membranes[64]. Eight proteins involved in
587 cristae formation were differentially expressed in our study: APOO (MIC26), APOOL

588 (MIC27), CHCHD3 (MIC19), and MIC60 from the MICOS complex; MTX1 and MTX2
589 from the SAM complex; TMEM11, a protein associating with multiple MICOS subunits for
590 cristae biogenesis[65]; and OMA1, a mitochondrial protease regulating OPA1[66] - a key protein
591 implicated in cristae remodelling[67] (Fig. 5; Supplementary Table 7). Seven of these proteins,
592 which almost entirely grouped within cluster-6 (Supplementary Fig. 3b and c; Supplementary
593 Table 6), were significantly decreased post-HVT, with four being decreased post-RVT
594 (Supplementary Table 8). To our knowledge, this is the first study to report a training-
595 induced de-prioritisation of these proteins. This is consistent with the minimal changes
596 observed in cristae density following short-term (< 3 months) exercise training in obese
597 individuals[68]. Thus, our results support the notion that cristae remodelling is not a priority
598 during short-term training and that changes in other mitochondrial proteins are more
599 important to adapt to the higher metabolic demand of exercise. Despite MICOS-MIB
600 subunits being known to interact with CLs[69], we report no correlation between the levels of
601 MICOS-MIB subunits and changes in CLs content following different training volumes.

Conclusions

Although endurance training has long been known to promote mitochondrial adaptations in skeletal muscle[6,7], and much progress has been made in the understanding of training-induced mitochondrial biogenesis[9,16], many of the underlying adaptive processes remain unknown or poorly understood. The present study addressed this fundamental gap by combining classic biological analyses with a multi-omics approach, enabling the elucidation of many novel adaptations to exercise training in humans. Our study demonstrated a training volume-dependent increase in mitochondrial respiration and enzyme activity, as well as OXPHOS protein content and SC formation. These adaptations were driven by an overall increase in mitochondrial content, consistent with previous observations[9,16-18]. However, using our strategy to normalise for changes in mitochondrial content we have unravelled an intricate and previously undemonstrated network of differentially prioritised mitochondrial adaptations; this demonstrated that training-induced changes in individual proteins, functional classes, and metabolic pathways are not stoichiometrically linked to the overall training-induced increase in mitochondrial content. Moreover, we provide evidence that the lack of stoichiometry and the differential prioritisation extended to all three levels (i.e., the transcriptome, proteome, and lipidome; Fig. 3a, 5, and 4e, respectively). This lack of stoichiometry was also evident between the levels investigated (e.g., between training-induced changes in the proteome and lipidome); while the largest number of changes in proteins took place early (post-NVT, Fig. 4b), no changes in lipid species were reported at this time point, rather occurring later in the intervention (Supplementary Fig. 4a). Finally, we demonstrated that the training stimulus associated with the RVT phase was sufficient to maintain almost all mitochondrial adaptations (with the exception of some changes in lipids). However, a main trend towards a generalised decrease can be observed at all three levels investigated, confirming the plasticity of skeletal muscle mitochondria[9]. This suggests that,

627 although a short taper (one week) may be sufficient to preserve previous gains, longer periods
628 of reduced training volume may indeed lead to a loss of mitochondrial adaptations[9,18].

629 As our data indicated that biochemical techniques (differential centrifugation) can only
630 enrich, but not purify, the mitochondrial extracts, we introduced a second (statistical)
631 normalisation layer. This, in combination with the power of a multi-omics approach, removed
632 the bias introduced by the overall training-induced increase in mitochondrial content and
633 enabled us to unearth the elaborate and complex remodelling taking place within
634 mitochondria. To the best of our knowledge, this is the first study investigating training-
635 induced changes in individual proteins and protein functional classes relative to the overall
636 increase in mitochondrial content. A striking and unexpected finding was the early (post-
637 NVT) deprioritisation in the formation of OXPHOS subunits. This suggests that exercise
638 training induces an increase in the biogenesis and proliferation of mitochondria that is greater
639 than the increase in the components of the OXPHOS machinery. Despite this deprioritisation
640 of OXPHOS subunits, mitochondrial respiration was enhanced with training - a feature that
641 was likely supported by the inherent reserve capacity of mitochondria (i.e., their ability to
642 respond to sudden increases in energy requirements)[70]. This could also be explained by the
643 lengthy time requirements necessary to assemble large multi-protein complexes[51];
644 nonetheless, this is unlikely, as the relative amount of OXPHOS subunits remained reduced
645 throughout the intervention, which lasted several weeks. The deprioritisation of OXPHOS
646 subunits becomes even more striking when considering that both TCA cycle and FAO
647 processes, two of the main suppliers of reducing equivalents to the OXPHOS system, were
648 upregulated early (post-NVT) and remained upregulated throughout. This is consistent with
649 the presence of a mitochondrial reserve capacity in human skeletal muscle of healthy
650 individuals[70] and indicates that enhancing electron flow to OXPHOS is more important to
651 increase ATP production than an increase in the components of the OXPHOS machinery.

This seems to also be confirmed by the relative decrease in proteins important for both CoQ biosynthesis and cristae formation (Fig. 5). Finally, the stoichiometric relationship between training-induced changes in OXPHOS SCs and mitochondrial content, which led to unchanged mt-specific mitochondrial respiration, adds to the growing evidence suggesting that SC formation does not confer enhancements in mitochondrial bioenergetics[28], at least not in human skeletal muscle of young individuals, as has been previously suggested[27].

In conclusion, our research demonstrates a complex network of non-stoichiometric mitochondrial adaptations to exercise training and highlights the elaborate and multi-layered nature of the adaptive response to exercise. This complexity was the result of changes in only one of the several programming variables of the exercise prescription (i.e., training volume). Future research utilising a similar approach is required to investigate the effects of manipulating other programming variables (e.g., exercise intensity, frequency, recovery between sessions) and the type of exercise (e.g., cycling, running, swimming, resistance training). These interventions are likely to induce adaptations that are specific and most likely different from the one presented in this research. Because of the well-documented therapeutic benefits of exercise training[71,72], the knowledge generated by our novel findings, which are readily available in supplemental tables, together with the results from future research, could subsequently be mined by medical practitioners and physicians. This would provide a valuable resource on how to manipulate exercise programming variables to tailor make programs aimed at obtaining specific mitochondrial adaptations in a personalised manner.

Methods

Participants and ethics approval. Ten healthy men volunteered to take part in this study (physiological and performance parameters are presented in Supplementary Table 1). Potential participants were deemed suitable if aged 18-35 y, were moderately-trained (i.e., less than 4 h per week of unstructured aerobic activity for half a year prior to the study), not regularly engaged in cycling-based sports, and were non-smokers and medication free prior to and during the study. Participants underwent a medical screening to exclude conditions that may have precluded their participation (e.g., cardiovascular, musculoskeletal and/or metabolic problems), and were informed of the study requirements, risks, and benefits, before giving written informed consent. Approval for the study's procedures, which conformed to the standards set by the latest revision of the Declaration of Helsinki, was granted by the Victoria University Human Research Ethics Committee (HRE15-126).

Study design. The study consisted of three consecutive training phases: the normal- (NVT), high- (LVT), and reduced- (RVT) training volume phase (Fig. 1a). Each training phase was preceded (and followed) by performance testing, which included a 20-km cycling time trial (20k-TT), a graded exercise test (GXT) (participants were previously familiarised with both tests), and a resting muscle biopsy. Overall study duration was ~9 weeks.

Testing procedures. Participants were required to avoid any vigorous exercise for the 48 h preceding each performance test (72 h for the skeletal muscle biopsy), from alcohol and any exercise for 24 h before testing, and from food and caffeine consumption for the 2 h preceding each test. Similar tests were performed at the same time of the day throughout the study to avoid variations caused by changes in circadian rhythm.

694 *GXT.* A graded exercise test was performed on an electronically-braked cycle ergometer
695 (Lode Excalibur v2.0, Groningen, The Netherlands) to determine peak oxygen uptake
696 ($\dot{V}O_{2Peak}$), peak power output ($\dot{W}_{Peak}$), the power attained at the lactate threshold ($\dot{W}_{LT}$) using
697 the modified D_{Max} method[73], and the training intensity for each training phase. The test
698 consisted of consecutive 4-min stages at constant power output; the test starting intensity
699 (range: 45-77 W) and the intensity increase of each stage (range: 17-28 W) were chosen so as
700 to obtain at least 8 time points for the determination of the $\dot{W}_{LT}$[74] and were based on
701 participants' fitness levels. An identical protocol was used at all 4 time points for each
702 participant. Prior to the test, and in the last 30 s of each stage, venous blood samples were
703 taken for measurement of blood lactate concentration ($[La^-]$). Participants were instructed to
704 keep a cadence > 60 rpm and were only allowed access to cadence. The test was stopped
705 when a participant reached volitional exhaustion or cadence dropped below 60 rpm for over
706 10 s. The $\dot{W}_{Peak}$ was determined as the power of the last completed stage plus an additional
707 25% of the stage increase wattage for every additional minute completed. At the end of each
708 GXT, after a 5-min recovery, a verification exhaustive bout was performed at an intensity
709 equivalent to $\dot{V}O_{2Peak}$ to confirm the highest measured $\dot{V}O_{2Peak}$[74]

710 *20k-TT.* Cycling time trials were performed on an electronically-braked cycle ergometer
711 (Velotron, RacerMate, Seattle, WA, USA) after a 6-min cycling warm-up (4 min at 66% of
712 $\dot{W}_{LT}$ followed by 2 min at $\dot{W}_{LT}$), and 2 min of rest. Participants were only allowed access to
713 cadence and completed distance.

714 *Gas Analysis during the GXT.* During the GXT, expired air was continuously analysed for O_2
715 and CO_2 concentrations via a gas analyser (Moxus 2010, AEI Technologies, Pittsburgh, PA,
716 USA), which was calibrated immediately before each test. $\dot{V}O_2$ values were recorded every
717 15 s and the average of the two highest consecutive 15-s values was recorded as a

718 participant's $\dot{V}O_{2Peak}$.

719 *Venous blood sampling.* Venous blood samples (~1 mL) were collected during the GXT from
720 a cannula inserted in the antecubital vain for the determination of venous blood [La^-] using a
721 blood-lactate analyser (2300 STAT Plus; YSI, Yellow Spring, OH, USA).

722 *Muscle biopsies.* A biopsy needle with suction under local anaesthesia (1% xylocaine) was
723 used to obtain vastus lateralis muscle biopsies at rest at the following four time points: BL,
724 PN, PH and PR. After being cleaned of excess blood, connective and fat tissue muscle
725 biopsies were divided as follows: ~10 mg was immediately immersed in ~2 mL of ice-cold
726 BIOPS for measurements of mitochondrial respiration, whereas the remainder was promptly
727 frozen in liquid nitrogen and stored at -80°C for follow-up analyses.

728 ***Training intervention.*** All training sessions were performed on an electronically braked
729 cycle ergometer (Velotron, RacerMate, USA), following an 8-min warm up (see 20k-TT) and
730 consisted of HIIT (2:1 work-to-rest ratio). Training intensity was set relative to $\dot{W}_{LT}$ (rather
731 than $\dot{W}_{Peak}$) so as to induce similar metabolic and cardiac stresses amongst participants of
732 differing fitness levels[75]. Exercise intensity was maintained between $\dot{W}_{LT}$ and $\dot{W}_{Peak}$
733 throughout the entire study so that training volume was the only manipulated variable
734 between the 3 phases.

735 *NVT phase.* This consisted of 6 HIIT sessions within 2 weeks of 5 to 7 4-min cycling
736 intervals interspersed with a 2-min recovery at 60 W. Exercise intensities were defined as
737 $[\dot{W}_{LT} + x(\dot{W}_{Peak}-\dot{W}_{LT})]$, with x increasing from 0.5 to 0.7 throughout the phase.

738 *HVT phase.* Participants performed HIIT twice a day for 20 consecutive days; training
739 sessions consisted of either 7 to 10 4-min intervals interspersed with a 2-min recovery at 60

W at intensities ranging from [$\dot{W}_{LT}$ + 0.5($\dot{W}_{Peak}$-$\dot{W}_{LT}$)] to [$\dot{W}_{LT}$ + 0.8($\dot{W}_{Peak}$-$\dot{W}_{LT}$)], or 15 to 20 2-min intervals at intensities ranging from [$\dot{W}_{LT}$ + 0.5($\dot{W}_{Peak}$-$\dot{W}_{LT}$)] to [$\dot{W}_{LT}$ + 0.95($\dot{W}_{Peak}$-$\dot{W}_{LT}$)], interspersed with a 1-min recovery at 60 W. Single session duration increased from ~45 min to 60 min.

RVT phase. The RVT phase consisted of 6 HIIT sessions in 6 days; participants performed 10, 9, 8, 7, 6, and 4, 4-min intervals interspersed with a 2-min recovery at 60 W, at an intensity of [$\dot{W}_{LT}$ + x($\dot{W}_{Peak}$- $\dot{W}_{LT}$)], with x increasing from 0.5 to 0.7 throughout the phase.

Physical activity and nutritional control. Physical activity and dietary patterns were maintained throughout the study and were monitored with the use of food and physical activity recall diaries. The last 3 meals prior to each performance test undertaken during baseline testing were recorded by each participant and were replicated thereafter before the same type of test. To control for dietary effects on muscle metabolism, participants were provided with a standardised dinner (55 kJ kg^{-1} body mass (BM), providing 2.1 g carbohydrate (CHO) kg^{-1} BM, 0.3 g fat kg^{-1} BM, and 0.6 g protein kg^{-1} BM) and breakfast (41 kJ kg^{-1} BM, providing 1.8 g CHO kg^{-1} BM, 0.2 g fat kg^{-1} BM, and 0.3 g protein kg^{-1} BM), to be consumed 15 and 3 h prior to the muscle biopsy, respectively.

Muscle analyses

Enzymatic activity. Enzyme activities were determined spectrophotometrically in post-600g supernatants of skeletal muscle homogenates according to the method described for respiratory chain complexes I-IV and citrate synthase[76]. Briefly, ~20mg of skeletal muscle sample was homogenized in sucrose/mannitol containing buffer using a glass/glass homogenizer and spun for 10 min at 600 g and 4 °C. The supernatant was then subjected to two freeze/thaw cycles and stored at -80 °C until measurement of respiratory chain enzymes.

763 CI was assayed as rotenone-sensitive NADH:CoQ1 oxidoreductase by monitoring the
764 decrease in absorbance due to NADH oxidation at 340 nm. For CII, activity was measured as
765 succinate:CoQ1 oxidoreductase by measuring CoQ1 reduction at 280 nm. CIII was assayed
766 as decylbenzylquinol; cytochrome *c* oxidoreductase by following the increase in absorbance
767 resulting from cytochrome *c* reduction at 550 nm. CIV was measured as cytochrome *c*
768 oxidase by following the decrease in absorbance resulting from cytochrome *c* oxidation at
769 550 nm. To assay the CS catalysed production of coenzyme A (CoA.SH) from oxaloacetate,
770 the generation of free sulfhydryl groups was monitored using the thiol reagent 5,5'-dithio-bis-
771 (2-nitobenzoic acid) (DTNB), which reacts spontaneously with the sulfhydryl groups to
772 produce 5-thio-2-nitrobenzoate anions. CS specific activity was measured by following the
773 increase in absorbance resulting from the formation of 5-thio-2 nitrobenzoate anions at
774 412nm. Following the enzyme measurements, the amount of protein in each sample was
775 determined using a bicinchoninic acid assay and activity calculated as initial rates (complexes
776 I, II and citrate synthase) or as first-order rate constants (complexes III and IV).

777 *Preparation of whole-muscle lysates for SDS-PAGE assessment of ETC subunits.* Frozen
778 skeletal muscle samples (~10 mg) were homogenised in a TissueLyzer for 2x 2 min at
779 maximum speed in ice-cold lysis buffer (1:20 w/v) containing 50 mM Tris-HCl, 150 mM
780 NaCl, 1 mM EDTA, 1% NP-40 and a phosphatase/protease inhibitor (5872, Cell Signaling
781 Technology, Danvers, MA, USA). Homogenates were rotated end-over-end at 4 °C for 1 h
782 and protein concentration was determined in triplicate using a commercial colorimetric assay
783 (Bio-Rad Protein Assay kit-II, Australia).

784 *Mitochondrial isolation for SDS- and BN-PAGE assessment of ETC subunits, complexes and*
785 *SCs*. Frozen skeletal muscle samples (~30 mg) were homogenised with 2x 20 strokes in a
786 Potter-Elvehjem tissue grinder attached to a rotating drill (~1000 rpm) in 5 mL solution A (1

mM EDTA, 220 mM mannitol, 20 mM HEPES-KOH [pH=7.6], 70 mM sucrose, 2 mg/mL BSA, 0.5 mM PMSF) and spun at 800 g for 5 min at 4°C. The supernatant was collected, whereas the pellet was re-homogenised as above in 5 mL of solution A to maximise extraction. The two supernatants were mixed and further spun at 800 g for 5 min at 4°C. The ensuing supernatant was then spun at 10,000 g for 20 min at 4°C, and the pellet was resuspended in 200 uL of sucrose buffer (0.5 M sucrose, 10 mM HEPES-KOH [pH=7.6], 0.5 mM PMSF). Protein concentration was determined by the bicinchoninic acid method according to the manufacturer's instructions (BCA Protein Assay Kit, Pierce-Thermo Fisher Scientific, Melbourne, Australia). This measurement was used to generate Fig. 1c.

SDS-PAGE. Both whole-muscle lysates (7.5 µg) and mitochondrial isolates (5 µg) were separated by electrophoresis using 12 or 15% SDS-PAGE gels, as previously described[77], and blotted with a total OXPHOS (ab110411, Abcam, Cambridge, MA, USA) or with a single CI (ab110242, Abcam, Cambridge, MA, USA) antibody where separation with CIV was not optimal using the total OXPHOS antibody.

BN-PAGE. Mitochondrial isolates (6-15 µg) were separated by electrophoresis using 3-12% NativePAGE gels (Life Technologies Australia, Mulgrave, Australia) as previously described[78]. A 4 g/g digitonin/protein ratio was used for assessment of SCs. The following primary antibodies were used: NADH:ubiquinone oxidoreductase subunit A9 (NDUFA9; ab14713), ubiquinol-cytochrome *c* reductase core protein 2 (UQCRC2; ab14745), cytochrome *c* oxidase subunit IV (COX IV; ab14744) (all Abcam, Cambridge, MA, USA).

For both SDS- and BN-PAGE, protein bands were visualised using a Bio-Rad ChemiDoc imaging system and bands were quantified using Bio-Rad Image Lab 5.0 software (Bio-Rad laboratories, Gladesville, NSW, Australia). An internal standard (made of a mixture of all

samples) was loaded in each SDS- and BN-PAGE gel, and each lane was normalised to this value, to reduce gel-to-gel variability.

Fibre preparation for high-resolution respirometry. Fresh muscle fibres were mechanically separated in ice-cold BIOPS (in mM: 2.77 CaK_2EGTA, 7.23 K_2EGTA, 5.77 Na_2ATP, 6.56 $MgCl_2$, 20 taurine, 50 MES, 15 Na_2phosphocreatine, 20 imidazole and 0.5 dithiothreitol adjusted to pH 7.1[11], followed by permeabilization by gentle agitation for 30 min at 4°C in BIOPS containing 50 µg/mL of saponin, and 3 5-min washes in MiR05 (in mM, unless specified: 0.5 EGTA, 3 $MgCl_2$, 60 K-lactobionate, 20 taurine, 10 KH_2PO_4, 20 HEPES, 110 sucrose and 1 g/L BSA essentially fatty acid-free, pH 7.1)[11]. Mitochondrial respiration was measured in duplicate (from 2-3 mg wet weight of muscle fibres) in MiR05 at 37°C using the high-resolution Oxygraph-2k (Oroboros, Innsbruck, Austria). To avoid potential oxygen diffusion limitation, oxygen concentration was maintained between 270 and 480 nmol mL^{-1} by re-oxygenation via direct syringe injection of O_2.

Mitochondrial respiration protocol. The substrate-uncoupler-inhibitor titration (SUIT) protocol[11] used was as follows: 0.2 mM octanoylcarnitine and 2 mM malate ($[ETF]_L$: leak respiration state [L] in the absence of adenylates and limitation of flux by electron input through electron transfer flavoprotein [ETF]); 3 mM $MgCl_2$ and 5 mM ADP ($[ETF]_P$: maximal OXPHOS capacity [P] with saturating levels of ADP and limitation of flux by electron input through ETF); 5 mM pyruvate ($[ETF+CI]_P$: P with saturating levels of ADP and limitation of flux by convergent electron input through ETF + CI); 10 mM succinate ($[ETF+CI+II]_P$: P with saturating levels of ADP and limitation of flux by convergent electron input through ETF + CI + CII); 10 µM cytochrome *c* (outer mitochondrial membrane integrity test); 0.75-1.5 µM carbonyl cyanide 4-(trifluoromethoxy) phenylhydrazone (FCCP) via stepwise titration ($[ETF+C+II]_E$, maximal electron transport chain capacity [E] with

saturating levels of ADP and limitation of flux by convergent electron input through ETF + CI + CII); 0.5 µM rotenone ([CII]$_E$: E with saturating levels of ADP and limitation of flux by electron input through CII); 5 µM antimycin A (residual non-mitochondrial oxygen consumption [ROX]). Data are presented as mass-specific mitochondrial respiration [pmol O_2 s^{-1} mg^{-1} wet weight] and as mitochondrial-specific respiration [pmol O_2 s^{-1} mg^{-1} wet weight/CS activity].

RNA-seq analysis. Approximately 10 to 15 mg of frozen muscle was used to isolate RNA using the RNeasy Mini Kit (Qiagen, Canada) according to the manufacturer's instructions. Samples were homogenised using the TissueLyser II (Qiagen, Canada). RNA concentration and purity were determined spectrophotometrically (NanoDrop 2000, Thermo Fisher Scientific, Wilmington, DE, USA) at 260 and 280 nm. RNA integrity was assessed using an Agilent Bioanalyzer according to manufacturer's instructions. The RNA was stored at -80 °C.

Sequencing and assembly of RNA-seq. This analysis was conducted on n = 5 participants (20 samples in total); samples were sequenced (100 base pair, single reads) on the Illumina NovaSeq 6000 platform at the Australian Genome Research Facility (AGRF). Transcriptome assembly was completed at AGRF with reads screened for presence of any Illumina adapter/overrepresented sequences and cross-species contamination. Per base sequence quality for all samples was >96% bases above Q30. Cleaned sequence reads were aligned against the *Homo sapiens* genome (Build version HG38). The STAR aligner (v2.5.3a) was used to map reads to the genomic sequences. Count of read mapping to each known gene were summarised to provide the matrix used for further analysis.

Bioinformatic analysis of RNA-seq data. For downstream RNA-seq analysis the R package *limma*[79] was used to conduct the differential expression analysis from count data. Count data

was normalised using calcNormFactors in the *edgeR* package in R. Differential expression analysis was performed between each subsequent biopsy to show comparative changes between each of the training volumes, though all comparisons were accounted for within the analysis. The resulting differential expression values were filtered for an adjusted *P* value < 0.05 using the Benjamini Hochberg method. Heatmaps were visualised using hierarchical clustering using the "average" method. Categorical columns for the generation of Fig. 3a were determined by identifying the transcripts to known descriptions in the literature; MICOS[80], TCA cycle[81], SLC25A[47], Assembly Factors[82]. All differentially expressed transcripts were run through Enrichr (https://maayanlab.cloud/Enrichr/[83,84]) and the top biological processes were identified with a combined score sorting for Fig. 3c.

Mitochondrial isolation for proteomics and lipidomics assessment. Frozen skeletal muscle samples (~30 mg) were homogenised with 2x 20 strokes in a Potter-Elvehjem tissue grinder attached to a rotating drill (~1000 rpm) in 3 mL solution B (1 mM EDTA, 220 mM mannitol, 20 mM HEPES-KOH [pH=7.6], 70 mM sucrose, 0.5 mM PMSF) and spun at 1000 g for 5 min at 4°C. The supernatant was further spun at 12000 g for 10 min at 4°C, and the ensuing pellet was resuspended in 200 uL of sucrose buffer (0.5 M sucrose, 10 mM HEPES-KOH [pH=7.6]). Protein concentration was determined by the bicinchoninic acid method according to the manufacturer's instructions (BCA Protein Assay Kit, Pierce-Thermo Fisher Scientific, Melbourne, Australia). Two IM fractions per sample (50 ug each) were were spun at 12000 g for 10 min at 4°C; after removal of the supernatant, the pellets were stored frozen at -80°C for subsequent proteomics and lipidomics analysis.

Proteomics. IM fractions were prepared for proteomics analysis as previously described[85] with minor modifications. Briefly, 50 µg of frozen mitochondrial isolates were solubilised in 20 µL of 8 M urea, 40 mM chloroacetamide, 10 mM tris(2-carboxyethyl)phosphine, 100 mM

Tris, pH 8.1; this was followed by 15 min of sonication in a water bath sonicator and 30 min of shaking (1500 rpm, at 37°C). The urea concentration was reduced to 2 M with H_2O prior to protein digestion with trypsin (Promega, Alexandria, NSW, Australia) at a 1:60 trypsin:protein ratio and subsequent overnight digestion at 37°C. The next day, samples were acidified with trifluoroacetic acid (1% [v/v] final concentration) and centrifuged for 5 min at 20,100 g at RT. The supernatants were desalted on pre-activated (100% acetonitrile [ACN]) and pre-equilibrated (0.1% TFA, 2% ACN) styrene divinylbenzene (SDB-XC; Supelco, Merck, Bayswater, VIC, Australia) stage tips[86] made in-house, before being washed (0.1% TFA, 2% ACN) and eluted in 0.1% TFA, 80% ACN. Samples were concentrated under vacuum and reconstituted in 0.1% TFA, 2% ACN. After 15 min sonication and subsequent vortexing samples were centrifuged at 20,100 g at RT before estimation of peptide concentration (Direct Detect, Merck). Approximately 600-800 ng of peptides were analysed on a Thermo Q Exactive™ Plus mass spectrometer coupled to an Ultimate 3000 HPLC (both Thermo Fisher Scientific, Mulgrave, VIC, Australia). Peptides were first loaded onto a trap column (Dionex-C18, 100 Å, 75 µm x 2 cm; Thermo Fisher Scientific) at an isocratic flow of 5 µL min^{-1} of 2% (v/v) ACN containing 0.1 % (v/v) formic acid (FA) for 5 min before switching the trap-column in line with the analytical column (Dionex-C18, 100 Å, 75 µm x 50 cm; Thermo Fisher Scientific). The separation of peptides was performed at 300 nL min^{-1} using a nonlinear ACN gradient of buffer A (2% ACN, 0.1% FA) and buffer B (80% ACN, 0.1% FA) over 125 min including void and equilibration. Data were collected in positive mode using Data Dependent Acquisition using m/z 375–1400 as MS scan range, HCD for MS/MS of the 15 most intense ions with $z \geq 2$. Other instrument parameters were: MS1 scan at 70,000 resolution (at 200 m/z), MS maximum injection time 50 ms, AGC target 3e6, stepped normalised collision energy of 27, 30, 32, isolation window of 1.6 m/z, MS/MS

905 resolution 17,500, MS/MS AGC target of 5e4, MS/MS maximum injection time 50 ms,
906 minimum intensity was set at 2e3 and dynamic exclusion was set to 30 s.

907 Raw files were analysed using the MaxQuant platform[87] version 1.6.1.0, searching against the
908 Uniprot human database containing reviewed, canonical variants in FASTA format (June
909 2018) and a database containing common contaminants by the Andromeda search engine[88].
910 Default search parameters for a label free quantification (LFQ) experiment were used with
911 modifications. In brief, "Label free quantification" was set to "LFQ" using a minimum ratio
912 count of 2. Cysteine carbamidomethylation was used as a fixed modification, and N-terminal
913 acetylation and methionine oxidation were used as variable modifications. False discovery
914 rates of 1% for proteins and peptides were applied by searching a reverse database, and
915 'match from and to', 'match between runs' options were enabled with a match time window
916 of 0.7 min. Unique and razor peptides with a minimum ratio count of 2 were used for
917 quantification.

918 *Bioinformatic analysis of proteomics data.* The R package *limma*[79] was used to conduct the
919 differential expression analysis of MaxQuant LFQ intensities (extracted from
920 proteinGroups.txt) after first performing normalisation using variance stabilising
921 normalisation (VSN) as found in the *limma* package. Identifications labelled by MaxQuant as
922 'only identified by site', 'reverse' and 'potential contaminant' were removed. Proteins having
923 less than 70% valid values were removed and remaining missing data was imputed using
924 QRILC method from the *imputeLCMD* package in R[89]. Differential expression analysis was
925 performed between BL and then each subsequent time point to show comparative changes
926 between each of the training volumes, though all comparisons were accounted for within the
927 analysis. Linear modelling was determined using eBayes in the *limma* package. The resulting
928 differential expression values were filtered for an adjusted P value < 0.01 using the

Benjamini Hochberg method. For the mitochondrial normalisation, all "Known Mitochondrial" proteins identified using the Integrated Mitochondrial Protein Index (IMPI)[8] were subset from the rest of the dataset, and then followed the normalisation and statistical validation as described above. Heatmaps were produced using hierarchical clustering using the "complete" method. Gene ontology of the clusters was determined by taking the proteins identified in the cluster and performing an enrichment analysis using the ClueGO (v2.5.6) application in Cytoscape (v3.7.1) using default settings except for a GO tree interval of 3 to 5, with only the Biological Processes Ontology switched on (Fig. 3d and Supplementary Fig. 3b). Full tables of identified proteins and post-normalisation differentially expressed proteins in their respective clusters and their annotations can be found in Supplementary Table 4 to 8.

The heatmaps presented in Fig. 5 and discussed in the Results section were generated according to Reactome pathways and/or literature searches (Supplementary Table 7). Proteins involved in two or more pathways were either presented in both pathways, or were assigned to the pathway involving the protein's primary function and/or most closely matching their training-induced changes. Specifically, "mitochondrial translation" was based on Reactome pathway R-HSA:5368287 (Mitochondrial translation). "TCA cycle" was based on Reactome pathway "R-HSA:71403 (Citric acid cycle [TCA cycle]); NNT was removed because its main physiological function is the generation of NADPH[90]. "FAO" was based on Reactome pathway R-HSA:556833 (Metabolism of Lipids); ETFA[91], ETFB[91], HSD17B10[92], and PLIN5[45] were added based on their involvement with FAO and lipid metabolism; GPD2[48,93], GPX1 (R-HSA-3299685 and[49]), and GPX4[49] where not presented within this pathway as their primary function suggested their inclusion in different pathways of Fig. 5; SAR1B was removed because its main function is the regulation of vesicle budding[94]. "OXPHOS" was based on Reactome pathway R-HSA:1632000 (Respiratory electron transport, ATP synthesis by chemiosmotic coupling, and heat production by uncoupling proteins); ETFA[91], ETFB[91],

ETFDH[48], TRAP1[52], and CYCS (R-HSA-3299685) were not presented within this pathway as their primary function and/or training-induced changes suggested their inclusion in different pathways of Fig. 5 was more appropriate; based on the main function of its constituent proteins the "OXPHOS" pathway was then subdivided in 2 subgroups: "OXPHOS - subunits", to which MP68[95] was added, and "OXPHOS - Assembly factors" to which ATPAF1[12], BCS1L[12], and COA3[12] were added. "Response to ROS" was based on Reactome pathway: R-HSA-3299685 (Detoxification of Reactive Oxygen Species); GPX4 was added based on its ability to reduce H_2O_2[49]. "Protein Folding" was based on literature searches: TRAP1, HSPA9, HSPD1, HSPE1, and TIMM44 were all added based on their involvement in protein folding and quality control mechanisms[52]. "CoQ biosynthesis" was based on Reactome pathway R-HSA-2142789 (Ubiquinol biosynthesis). "CoQ e- donors" was based on literature searches: DHODH[48], ETFDH[48], GPD2[48], IVD[61], DLD[62] and L2HGDH[63], were all added based on their function to feed electrons into the respiratory chain via CoQ. "Cristae formation" was based on Reactome pathway R-HSA-8949613 (Cristae formation); OMA1[66,67] was added based on its involvement in cristae formation, whereas ATP5A1, ATP5J, ATP5B, ATP5H, and ATP5O (all based on R-HSA:163200), as well as HSPA9[52] were not presented within this pathway as their primary function suggested their inclusion in different pathways of Fig. 5.

Lipid extraction for lipidomics. Mitochondrial isolates were extracted using a modified single-phase chloroform/methanol extraction as described previously[96]. In brief, 20 volumes of chloroform:methanol (2:1) were added to the sample along with a series of internal standards. Samples were vortexed and centrifuged on a rotary mixer for 10 min. Following sonication on a sonicator bath for 30 min, samples were rested for 20 min prior to centrifugation at 13,000 g for 10 min. Supernatants were transferred into a 96 well plated, dried down and reconstituted in 50 µL H_2O saturated butanol and sonicated for 10 min. After

the addition of 50 µL of methanol with 10 mM ammonium formate, samples were centrifuged at 4000 rpm on a plate centrifuge and transferred into glass vials with inserts for mass spectrometry analysis.

Targeted lipidomics analysis. LC-MS/MS was performed according to previously published methods, with slight modification for tissue samples[97]. Sample extracts were analysed using either (i) an AB Sciex Qtrap 4000 mass spectrometer coupled to an Agilent 1200 HPLC system for CL assessment, as described preciously[98] or (ii) an Agilent 6490 QQQ mass spectrometer coupled with an Agilent 1290 series HPLC system for assessment of all other lipid species[97]. Lipids run on the Agilent 6490 were measured using scheduled multiple reaction monitoring with the following conditions: isolation widths for Q1 and Q3 were set to "unit" resolution (0.7 amu), gas temperature 150°C, nebulizer 20 psi, sheath gas temperature 200°C, gas flow rate 17 L/min, capillary voltage 3500 V and sheath gas flow 10 L/min. The list of MRMs used and the chromatographic conditions were described previously[97].

Bioinformatic analysis of lipidomics data. For lipidomics we identified that the increase in CLs in the un-normalised data was due to a training-induced increase in MPE in our mitochondrial isolates. To eliminate this bias, all lipid species were normalised by total CL amount (Supplementary Table 9). Lipid species were log transformed before undergoing differential expression analysis in *limma*[79], with linear models using the eBayes function. The resulting differential expression values were filtered for an adjusted P value < 0.05 using Benjamini Hochberg method (Supplementary Table 10). Heatmaps were visualised using hierarchical clustering using the "complete" method. Profile plots were determined by taking the mean of the z-score for all participants' samples for each lipid species at each exercise volume (Fig. 4f). Higher classes were determined through descriptions of the literature as assigned by the Lipid Metabolites and Pathways Strategy (Lipid MAPS)[99].

Statistical Analysis. All values are reported as means ± SD, unless otherwise specified. For non-omics analyses: outliers were first removed using the ROUT method set at Q = 1%[100]. Normally distributed datasets (Shapiro-Wilk test $P > 0.05$) were analysed by a repeated measures one-way ANOVA followed by Tukey's correction post hoc testing. Non-normally distributed datasets (Shapiro-Wilk test $P < 0.05$) were transformed using, in order, log(Y), 1/Y, √Y, until normality was met, before being analysed as above; datasets that remained non-normal following 3 independent transformation attempts were analysed using the non-parametric Friedman test on the raw data followed by Dunn's correction post hoc testing. The level of statistical significance was set a priori at $P < 0.05$. GraphPad Prism (v. 8.4.2) was used for all statistical non-omics analyses.

Data availability. The R scripts used for all omics analyses described above are deposited on GitHub at https://github.com/XercisOmics/EnduranceMitoMultiOmics. Raw RNASeq and mass-spectrometry data will be uploaded to NCBI, ProteomeXchange and Metabolomics Workbench repositories upon publication.

Acknowledgments. We thank the participants for their time and commitment to this study. The authors would like to acknowledge all members of the Stroud and Bishop labs for input into interpretation and presentation of data. We thank the Bio21 Mass Spectrometry and Proteomics Facility (MMSPF) for provision of instrumentation, training, and technical support. We acknowledge the use of the services and facilities of the Australian Genome Research Facility (AGRF). This study was funded by grants from the ANZ-MASON Foundation (to D.J.B), the Australian Research Council (Discovery Project DP140104165 to D.J.B), the Australian National Health and Medical Research Council (NHMRC Project Grant 1140906 to D.A.S.; NHMRC Fellowships 1140851 to D.A.S. and 1155244 to D.R.T.), JDRF Australia (JDRF Career Development to M.T.C.), and the Australian Research Council Special Research Initiative in Type 1 Juvenile Diabetes (to M.T.C.). We acknowledge the support of the Mito Foundation for the provision of instrumentation and the Victorian Government's Operational Infrastructure Support Program.

Author contributions. C.G., D.A.S., and D.J.B. conceptualised the study. C.G., D.A.S., and D.J.B. devised the study methodology. C.G., N.A.J., and H.A.J. performed study validation. C.G., N.A.J, H.A.J. delivered the training and performed sample collection. C.G., J.B., J.K., B.R., A.L., T.L.S., and A.E.F. performed biochemical analyses. C.G., B.R., and D.A.S., performed proteomic analysis. K.H., and N.A.M. performed lipidomic analysis. RNA-seq analysis was performed at the Australian Genome Research Facility (AGRF). C.G., N.J.C., and D.A.S. performed statistical and bioinformatic analysis. C.G., N.J.C., and D.A.S. delivered the visualisation. C.G., D.A.S., and D.J.B. wrote the manuscript. M.T.C., P.J.M., D.R.T., D.A.S, and D.J.B. provided supervision. D.R.T., M.T.C., D.A.S, and D.J.B. funded the research. C.G., D.A.S., and D.J.B. have primary responsibility for final content. Data collection took place at Victoria University. Muscle analysis took place at Victoria University, Monash University, Murdoch Children's Research Institute, the Baker Heart &

1042 Diabetes Institute, AGRF, and the Bio21 Molecular Science & Biotechnology Institute (The
1043 University of Melbourne). All persons designated as authors qualify for authorship, and all
1044 those qualifying for authorship are listed. All authors have read and approved the final
1045 manuscript.

1046 **Competing interest.** The authors declare no conflict of interest.

References

1 Spinelli, J. B. & Haigis, M. C. The multifaceted contributions of mitochondria to cellular metabolism. *Nat. Cell Biol.* **20**, 745-754 (2018).

2 Gorman, G. S. *et al.* Mitochondrial diseases. *Nature reviews Disease primers* **2**, 1-22 (2016).

3 Lin, M. T. & Beal, M. F. Mitochondrial dysfunction and oxidative stress in neurodegenerative diseases. *Nature* **443**, 787-795 (2006).

4 López-Otín, C., Blasco, M. A., Partridge, L., Serrano, M. & Kroemer, G. The hallmarks of aging. *Cell* **153**, 1194-1217 (2013).

5 Nunnari, J. & Suomalainen, A. Mitochondria: in sickness and in health. *Cell* **148**, 1145-1159, doi:10.1016/j.cell.2012.02.035 (2012).

6 Holloszy, J. O. Biochemical adaptations in muscle. Effects of exercise on mitochondrial oxygen uptake and respiratory enzyme activity in skeletal muscle. *J. Biol. Chem.* **242**, 2278-2282 (1967).

7 Hoppeler, H., Lüthi, P., Claassen, H., Weibel, E. R. & Howald, H. The ultrastructure of the normal human skeletal muscle. *Pflügers Archiv* **344**, 217-232, doi:10.1007/bf00588462 (1973).

8 Smith, A. C. & Robinson, A. J. MitoMiner v4. 0: an updated database of mitochondrial localization evidence, phenotypes and diseases. *Nucleic Acids Res.* **47**, D1225-D1228 (2019).

9 Granata, C., Jamnick, N. A. & Bishop, D. J. Training-induced changes in mitochondrial content and respiratory function in human skeletal muscle. *Sports Med.* **48**, 1809–1828 (2018).

10 Granata, C., Jamnick, N. A. & Bishop, D. J. Principles of exercise prescription, and how they influence exercise-induced changes of transcription factors and other regulators of mitochondrial biogenesis. *Sports Med.* **48**, 1541–1559 (2018).

11 Pesta, D. & Gnaiger, E. in *Mitochondrial Bioenergetics: Methods and Protocols* Vol. 810 (eds Carlos M. Palmeira & Antonio J. Moreno) 25-58 (Springer Science+Business Media, 2012).

12 Signes, A. & Fernandez-Vizarra, E. Assembly of mammalian oxidative phosphorylation complexes I–V and supercomplexes. *Essays Biochem.* **62**, 255-270 (2018).

13 Greggio, C. *et al.* Enhanced respiratory chain supercomplex formation in response to exercise in human skeletal muscle. *Cell Metab.* **25**, 301-311 (2017).

14 Wyckelsma, V. L. *et al.* Preservation of skeletal muscle mitochondrial content in older adults: relationship between mitochondria, fibre type and high-intensity exercise training. *The Journal of physiology* **595**, 3345-3359 (2017).

15 Ørtenblad, N. Mitochondrial increase in volume density with exercise training: More, larger or better? *Acta Physiologica* **222**, e12976 (2018).

16 Bishop, D. J. *et al.* High-Intensity Exercise and Mitochondrial Biogenesis: Current Controversies and Future Research Directions. *Physiology* **34**, 56-70, doi:10.1152/physiol.00038.2018 (2019).

17 Bishop, D. J., Granata, C. & Eynon, N. Can we optimise the exercise training prescription to maximise improvements in mitochondria function and content? *Biochim. Biophys. Acta, Gen. Subj.* **1840**, 1266-1275 (2014).

18 Granata, C., Oliveira, R. S. F., Little, J. P., Renner, K. & Bishop, D. J. Mitochondrial adaptations to high-volume exercise training are rapidly reversed after a reduction in training volume in human skeletal muscle. *FASEB J.* **30**, 3413-3423, doi:10.1096/fj.201500100R (2016).

19 Larsen, S. *et al.* Biomarkers of mitochondrial content in skeletal muscle of healthy young human subjects. *J. Physiol.* **590**, 3349-3360 (2012).

20 Barnard, R. J., Edgerton, V. R. & Peter, J. Effect of exercise on skeletal muscle. I. Biochemical and histochemical properties. *J. Appl. Physiol.* **28**, 762-766 (1970).

21 Golinick, P. D., Ianuzzo, C. D. & King, D. W. in *Muscle metabolism during exercise* 69-85 (Springer, 1971).

22 Morgan, T., Cobb, L., Short, F., Ross, R. & Gunn, D. in *Muscle metabolism during exercise* 87-95 (Springer, 1971).

23 Little, J. P. *et al.* Low-volume high-intensity interval training reduces hyperglycemia and increases muscle mitochondrial capacity in patients with type 2 diabetes. *J. Appl. Physiol.* **111**, 1554-1560, doi:10.1152/japplphysiol.00921.2011 (2011).

24 Tonkonogi, M. & Sahlin, K. Rate of oxidative phosphorylation in isolated mitochondria from human skeletal muscle: Effect of training status. *Acta Physiol. Scand.* **161**, 345-353 (1997).

25 Meinild Lundby, A. K. *et al.* Exercise training increases skeletal muscle mitochondrial volume density by enlargement of existing mitochondria and not de novo biogenesis. *Acta Physiol* **222**, e12905, doi:10.1111/apha.12905 (2018).

26 Schägger, H. & Pfeiffer, K. Supercomplexes in the respiratory chains of yeast and mammalian mitochondria. *The EMBO journal* **19**, 1777-1783 (2000).

27 Lapuente-Brun, E. *et al.* Supercomplex assembly determines electron flux in the mitochondrial electron transport chain. *Science* **340**, 1567-1570 (2013).

28 Hirst, J. Open questions: respiratory chain supercomplexes—why are they there and what do they do? *BMC Biol.* **16**, 111 (2018).

29 Pillon, N. J. *et al.* Transcriptomic profiling of skeletal muscle adaptations to exercise and inactivity. *Nature communications* **11**, 1-15 (2020).

30 Calvo, S. E., Clauser, K. R. & Mootha, V. K. MitoCarta2.0: an updated inventory of mammalian mitochondrial proteins. *Nucleic Acids Res.* **44**, D1251-1257, doi:10.1093/nar/gkv1003 (2016).

31 Egan, B. *et al.* 2-D DIGE analysis of the mitochondrial proteome from human skeletal muscle reveals time course-dependent remodelling in response to 14 consecutive days of endurance exercise training. *Proteomics* **11**, 1413-1428 (2011).

32 Holloway, K. V. *et al.* Proteomic investigation of changes in human vastus lateralis muscle in response to interval-exercise training. *Proteomics* **9**, 5155-5174 (2009).

33 Hostrup, M., Onslev, J., Jacobson, G. A., Wilson, R. & Bangsbo, J. Chronic β2-adrenoceptor agonist treatment alters muscle proteome and functional adaptations induced by high intensity training in young men. *The Journal of physiology* **596**, 231-252 (2018).

34 Robinson, M. M. *et al.* Enhanced protein translation underlies improved metabolic and physical adaptations to different exercise training modes in young and old humans. *Cell Metab.* **25**, 581-592 (2017).

35 Ubaida-Mohien, C. *et al.* Physical activity associated proteomics of skeletal muscle: being physically active in daily life may protect skeletal muscle from aging. *Front. Physiol.* **10**, 312 (2019).

36 Christensen, P. M. *et al.* A short period of high-intensity interval training improves skeletal muscle mitochondrial function and pulmonary oxygen uptake kinetics. *J. Appl. Physiol.* **120**, 1319-1327 (2016).

37 Jacobs, R. A. *et al.* Improvements in exercise performance with high-intensity interval training coincide with an increase in skeletal muscle mitochondrial content and function. *J. Appl. Physiol.* **115**, 785-793, doi:10.1152/japplphysiol.00445.2013 (2013).

38 Paradies, G., Paradies, V., De Benedictis, V., Ruggiero, F. M. & Petrosillo, G. Functional role of cardiolipin in mitochondrial bioenergetics. *Biochimica et Biophysica Acta (BBA)-Bioenergetics* **1837**, 408-417 (2014).

39 Dube, J. *et al.* Effects of weight loss and exercise on insulin resistance, and intramyocellular triacylglycerol, diacylglycerol and ceramide. *Diabetologia* **54**, 1147-1156 (2011).

40 Shepherd, S. *et al.* Lipid droplet remodelling and reduced muscle ceramides following sprint interval and moderate-intensity continuous exercise training in obese males. *Int. J. Obes.* **41**, 1745 (2017).

41 Bruce, C. R. *et al.* Endurance training in obese humans improves glucose tolerance and mitochondrial fatty acid oxidation and alters muscle lipid content. *American Journal of Physiology - Endocrinology and Metabolism* **291**, E99-E107, doi:10.1152/ajpendo.00587.2005 (2006).

42 Perreault, L. *et al.* Intracellular localization of diacylglycerols and sphingolipids influences insulin sensitivity and mitochondrial function in human skeletal muscle. *JCI insight* **3** (2018).

43 Goodpaster, B. H. & Kelley, D. E. Role of muscle in triglyceride metabolism. *Curr. Opin. Lipidol.* **9**, 231-236 (1998).

44 Walther, T. C. & Farese Jr, R. V. Lipid droplets and cellular lipid metabolism. *Annu. Rev. Biochem.* **81**, 687-714 (2012).

45 Benador, I. Y., Veliova, M., Liesa, M. & Shirihai, O. S. Mitochondria bound to lipid droplets: where mitochondrial dynamics regulate lipid storage and utilization. *Cell Metab.* **29**, 827-835 (2019).

46 Wang, H. *et al.* Perilipin 5, a lipid droplet-associated protein, provides physical and metabolic linkage to mitochondria. *J. Lipid Res.* **52**, 2159-2168 (2011).

47 Palmieri, F. The mitochondrial transporter family SLC25: identification, properties and physiopathology. *Mol. Aspects Med.* **34**, 465-484 (2013).

48 Wang, Y. & Hekimi, S. Understanding ubiquinone. *Trends Cell Biol.* **26**, 367-378 (2016).

49 Powers, S. K. *et al.* Exercise-induced oxidative stress: Friend or foe? *Journal of sport and health science* (2020).

50 LaHue, S. C., Comella, C. L. & Tanner, C. M. The best medicine? The influence of physical activity and inactivity on Parkinson's disease. *Mov. Disord.* **31**, 1444-1454 (2016).

51 McKenzie, M., Lazarou, M., Thorburn, D. R. & Ryan, M. T. Analysis of mitochondrial subunit assembly into respiratory chain complexes using Blue Native polyacrylamide gel electrophoresis. *Anal. Biochem.* **364**, 128-137, doi:10.1016/j.ab.2007.02.022 (2007).

52 Voos, W. Chaperone–protease networks in mitochondrial protein homeostasis. *Biochimica et Biophysica Acta (BBA)-Molecular Cell Research* **1833**, 388-399 (2013).

53 Wiedemann, N. & Pfanner, N. Mitochondrial machineries for protein import and assembly. *Annu. Rev. Biochem.* **86**, 685-714 (2017).

54 Gebert, N. *et al.* Mitochondrial cardiolipin involved in outer-membrane protein biogenesis: implications for Barth syndrome. *Curr. Biol.* **19**, 2133-2139 (2009).

55 Pfeiffer, K. *et al.* Cardiolipin stabilizes respiratory chain supercomplexes. *J. Biol. Chem.* **278**, 52873-52880 (2003).

56 Ikon, N. & Ryan, R. O. Cardiolipin and mitochondrial cristae organization. *Biochimica et Biophysica Acta (BBA)-Biomembranes* **1859**, 1156-1163 (2017).

57 Malhotra, A., Xu, Y., Ren, M. & Schlame, M. Formation of molecular species of mitochondrial cardiolipin. 1. A novel transacylation mechanism to shuttle fatty acids between sn-1 and sn-2 positions of multiple phospholipid species. *Biochimica et Biophysica Acta (BBA)-Molecular and Cell Biology of Lipids* **1791**, 314-320 (2009).

58 Wang, Y. & Hekimi, S. The complexity of making ubiquinone. *Trends Endocrinol. Metab.* **30**, 929-943 (2019).

59 Stefely, J. A. & Pagliarini, D. J. Biochemistry of mitochondrial coenzyme Q biosynthesis. *Trends Biochem. Sci.* **42**, 824-843 (2017).

60 Svensson, M. *et al.* Effect of Q10 supplementation on tissue Q10 levels and adenine nucleotide catabolism during high-intensity exercise. *Int. J. Sport Nutr. Exerc. Metab.* **9**, 166-180 (1999).

61 Finocchiaro, G., Ito, M. & Tanaka, K. Purification and properties of short chain acyl-CoA, medium chain acyl-CoA, and isovaleryl-CoA dehydrogenases from human liver. *J. Biol. Chem.* **262**, 7982-7989 (1987).

62 Xia, L., Björnstedt, M., Nordman, T., Eriksson, L. C. & Olsson, J. M. Reduction of ubiquinone by lipoamide dehydrogenase: An antioxidant regenerating pathway. *Eur. J. Biochem.* **268**, 1486-1490 (2001).

63 Oldham, W. M., Clish, C. B., Yang, Y. & Loscalzo, J. Hypoxia-mediated increases in L-2-hydroxyglutarate coordinate the metabolic response to reductive stress. *Cell Metab.* **22**, 291-303 (2015).

64 Huynen, M. A., Mühlmeister, M., Gotthardt, K., Guerrero-Castillo, S. & Brandt, U. Evolution and structural organization of the mitochondrial contact site (MICOS) complex and the mitochondrial intermembrane space bridging (MIB) complex. *Biochimica et Biophysica Acta (BBA)-Molecular Cell Research* **1863**, 91-101 (2016).

65 Guarani, V. *et al.* QIL1 is a novel mitochondrial protein required for MICOS complex stability and cristae morphology. *Elife* **4**, e06265 (2015).

66 Ehses, S. *et al.* Regulation of OPA1 processing and mitochondrial fusion by m-AAA protease isoenzymes and OMA1. *J. Cell Biol.* **187**, 1023-1036 (2009).

67 Frezza, C., Cipolat, S. & Scorrano, L. Organelle isolation: functional mitochondria from mouse liver, muscle and cultured filroblasts. *Nat. Protoc.* **2**, 287, doi:10.1038/nprot.2006.478 (2007).

68 Nielsen, J. *et al.* Plasticity in mitochondrial cristae density allows metabolic capacity modulation in human skeletal muscle. *J. Physiol.* **595**, 2839-2847 (2017).

69 Weber, T. A. *et al.* APOOL is a cardiolipin-binding constituent of the Mitofilin/MINOS protein complex determining cristae morphology in mammalian mitochondria. *PLoS One* **8**, e63683 (2013).

70 Desler, C. *et al.* Is there a link between mitochondrial reserve respiratory capacity and aging? *Journal of aging research* **2012** (2012).

71 Booth, F. W., Gordon, S. E., Carlson, C. J. & Hamilton, M. T. Waging war on modern chronic diseases: primary prevention through exercise biology. *J. Appl. Physiol.* **88**, 774-787 (2000).

72 Pedersen, B. K. & Saltin, B. Evidence for prescribing exercise as therapy in chronic disease. *Scand. J. Med. Sci. Sports* **16**, 3-63 (2006).

73 Bishop, D. J., Jenkins, D. G., McEniery, M. & Carey, M. F. Relationship between plasma lactate parameters and muscle characteristics in female cyclists. *Med. Sci. Sports Exerc.* **32**, 1088-1093 (2000).

74 Jamnick, N. A., Botella, J., Pyne, D. B. & Bishop, D. J. Manipulating graded exercise test variables affects the validity of the lactate threshold and V˙ O2peak. *PLoS One* **13**, e0199794 (2018).

75 Baldwin, J., Snow, R. J. & Febbraio, M. A. Effect of training status and relative exercise intensity on physiological responses in men. *Med. Sci. Sports Exerc.* **32**, 1648-1654 (2000).

76 Frazier, A. E., Vincent, A. E., Turnbull, D. M., Thorburn, D. R. & Taylor, R. W. in *Methods Cell Biol.* Vol. 155 121-156 (Elsevier, 2020).

77 Granata, C., Oliveira, R. S. F., Little, J. P., Renner, K. & Bishop, D. J. Training intensity modulates changes in PGC-1α and p53 protein content and mitochondrial respiration, but not markers of mitochondrial content in human skeletal muscle. *FASEB J.* **30**, 959-970, doi:10.1096/fj.15-276907 (2016).

78 Jha, P., Wang, X. & Auwerx, J. Analysis of Mitochondrial Respiratory Chain Supercomplexes Using Blue Native Polyacrylamide Gel Electrophoresis (BN-PAGE). *Curr. Protoc. Mouse Biol.*, 1-14 (2016).

79 Ritchie, M. E. *et al.* limma powers differential expression analyses for RNA-sequencing and microarray studies. *Nucleic Acids Res.* **43**, e47-e47 (2015).

80 Eramo, M. J., Lisnyak, V., Formosa, L. E. & Ryan, M. T. The 'mitochondrial contact site and cristae organising system'(MICOS) in health and human disease. *The Journal of Biochemistry* **167**, 243-255 (2020).

81 Martínez-Reyes, I. & Chandel, N. S. Mitochondrial TCA cycle metabolites control physiology and disease. *Nature communications* **11**, 1-11 (2020).

82 Hock, D. H., Robinson, D. R. & Stroud, D. A. Blackout in the powerhouse: clinical phenotypes associated with defects in the assembly of OXPHOS complexes and the mitoribosome. *Biochem. J.* **477**, 4085-4132 (2020).

83 Chen, E. Y. *et al.* Enrichr: interactive and collaborative HTML5 gene list enrichment analysis tool. *BMC Bioinformatics* **14**, 128 (2013).

84 Kuleshov, M. V. *et al.* Enrichr: a comprehensive gene set enrichment analysis web server 2016 update. *Nucleic Acids Res.* **44**, W90-W97 (2016).

85 Stroud, D. A. *et al.* Accessory subunits are integral for assembly and function of human mitochondrial complex I. *Nature* **538**, 123 (2016).

86 Kulak, N. A., Pichler, G., Paron, I., Nagaraj, N. & Mann, M. Minimal, encapsulated proteomic-sample processing applied to copy-number estimation in eukaryotic cells. *Nature methods* **11**, 319 (2014).

87 Cox, J. & Mann, M. MaxQuant enables high peptide identification rates, individualized ppb-range mass accuracies and proteome-wide protein quantification. *Nat. Biotechnol.* **26**, 1367-1372 (2008).

88 Cox, J. *et al.* Andromeda: a peptide search engine integrated into the MaxQuant environment. *J. Proteome Res.* **10**, 1794-1805 (2011).

89 Lazar, C. imputeLCMD: A Collection of Methods for Left-Censored Missing Data Imputation. R package, version 2.0.

90 Kampjut, D. & Sazanov, L. A. Structure and mechanism of mitochondrial proton-translocating transhydrogenase. *Nature* **573**, 291-295 (2019).

91 Watmough, N. J. & Frerman, F. E. The electron transfer flavoprotein: ubiquinone oxidoreductases. *Biochimica et Biophysica Acta (BBA)-Bioenergetics* **1797**, 1910-1916 (2010).

92 Schulz, H. Beta oxidation of fatty acids. *Biochimica et Biophysica Acta (BBA)-Lipids and Lipid Metabolism* **1081**, 109-120 (1991).

93 Mráček, T., Drahota, Z. & Houštěk, J. The function and the role of the mitochondrial glycerol-3-phosphate dehydrogenase in mammalian tissues. *Biochimica et Biophysica Acta (BBA)-Bioenergetics* **1827**, 401-410 (2013).

94 Takai, Y., Sasaki, T. & Matozaki, T. Small GTP-binding proteins. *Physiol. Rev.* **81**, 153-208 (2001).

95 Fujikawa, M., Ohsakaya, S., Sugawara, K. & Yoshida, M. Population of ATP synthase molecules in mitochondria is limited by available 6.8-kDa proteolipid protein (MLQ). *Genes Cells* **19**, 153-160 (2014).

96 Weir, J. M. *et al.* Plasma lipid profiling in a large population-based cohort. *J. Lipid Res.* **54**, 2898-2908 (2013).

97 Huynh, K. *et al.* High-throughput plasma lipidomics: detailed mapping of the associations with cardiometabolic risk factors. *Cell chemical biology* **26**, 71-84. e74 (2019).

98 Tan, S. M. *et al.* Complement C5a Induces Renal Injury in Diabetic Kidney Disease by Disrupting Mitochondrial Metabolic Agility. *Diabetes* **69**, 83-98 (2020).

99 Fahy, E., Cotter, D., Sud, M. & Subramaniam, S. Lipid classification, structures and tools. *Biochimica et Biophysica Acta (BBA)-Molecular and Cell Biology of Lipids* **1811**, 637-647 (2011).

100 Motulsky, H. J. & Brown, R. E. Detecting outliers when fitting data with nonlinear regression–a new method based on robust nonlinear regression and the false discovery rate. *BMC Bioinformatics* **7**, 123 (2006).